2021-09

Forecasting coastal evolution on time-scales of days to decades

Mikhalenko, Natalia

10.1016/j.coastaleng.2021.103928
Coastal Engineering
Elsevier BV

Journal Pre-proof

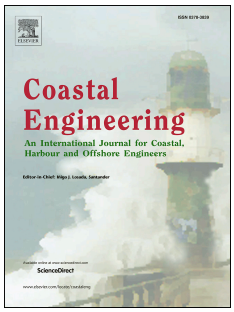

Forecasting coastal evolution on time-scales of days to decades.

Mark Davidson

PII: S0378-3839(21)00087-9

DOI: https://doi.org/10.1016/j.coastaleng.2021.103928

Reference: CENG 103928

To appear in: *Coastal Engineering*

Received Date: 19 October 2020

Revised Date: 12 May 2021

Accepted Date: 30 May 2021

Please cite this article as: Davidson, M., Forecasting coastal evolution on time-scales of days to decades., *Coastal Engineering* (2021), doi: https://doi.org/10.1016/j.coastaleng.2021.103928.

Forecasting coastal evolution on time-scales of days to decades.

Key words: Prediction, Coastal-evolution, Long-term, Forecasting, Equilibrium, Reduced-complexity.

Mark Davidson[1]

Abstract

Increasing pressures on coastal environments induced by sea level rise and coastal squeeze has meant that tracking the morphological evolution of sedimentary coasts from the last known survey, pre-empting storm impacts and forecasting potential beach recovery following extreme events is of substantial and increasing societal importance. Equilibrium models for forecasting coastal evolution have figured prominently in the literature in the past two decades and show a strong potential for fulfilling this societal need. In particular some very skilful shoreline evolution models have been proposed based on equilibrium concepts. These models are stable, simple and permit long-term (O(10) years) predictions of coastal change. However, equilibrium models are typically highly empirical and in many cases do not consider explicitly the impact of dynamic sea level, which is modulated by tides, surge and global sea level rise. Equilibrium-based models of shoreline evolution have shown particular promise, but these models generally do not consider the role of the sub- and supra- tidal morphology on coastal evolution (e.g. the importance of coastal dune systems). This contribution presents a new model for Forecasting Coastal Evolution (ForCE), which addresses these issues. The model algorithm adopts a reduced complexity but fundamentally physics-based approach, whilst maintaining equilibrium principles. Unlike, most prior models, the sub- and supra- tidal areas are represented explicitly in the model, as are sea level variations. Sediment transport is equated directly with the disequilibrium in wave energy dissipation flux, leading to a sediment transport formulation that negates the normal intermediate step of computing surfzone currents, generally required in process models. Two components of sediment transport are considered: The first is forced by the turbulent kinetic energy associated with wave breaking and the second diffusive term, is related to a sea bed-slope disequilibrium. The first component perturbs the equilibrium profile and dominates in the surfzone, whilst that latter component plays an important role in beach recovery. Equations are developed for a depth-averaged, beach profile model, assuming longshore uniformity. These computational efficient and stable equations facilitate long forecasts (>decade) and easy comparisons with a field data at cross-shore transport dominated field sites. At the test field site, the model is capable of reproducing qualitative observations of nearshore sand-bar dynamics and quantitative comparisons with measured coastal state indicators including both the shoreline displacement ($r = 0.90$, *N.M.S.E.* = 0.145) and intertidal beach volume ($r = 0.87$).

[1] Corresponding Author. Coastal Processes Research Group, Plymouth University, Drake Circus, Plymouth, Devon, PL4 8AA.

1. Introduction

On sedimentary coasts, mobile beach sediments provide a key role in dissipating incident wave energy and provide the essential freeboard to ameliorate wave overtopping and coastal flooding. Monitoring morphological change is a critical component of assessing coastal resilience to erosion, flooding and the potential for damage/loss of infrastructure. However, beach surveys are costly and rarely frequent enough to provide a good assessment of the current state of the coastline, nor do they provide estimates of the likely future state of the coastline due to storm impacts, or the subsequent probability of beach-recovery.

Numerical models potentially provide a means of bridging this capability gap. An established modelling approach is the application of detailed process-based models, (e.g., Mike 21, Delft 3D, XBeach or Telemac), which include the detailed physics of wave propagation, dissipation, generation of nearshore currents, sediment transport and the resulting morphological change and multiple feedback loops (Warren and Bach, 1992; Lesser et al., 2004; Roelvink et al., 2009; Villaret et al., 2013). This modelling genre has proved very successful in predicting plethora of nearshore phenomena including storm/dune erosion and wave overtopping. However, process models are computationally demanding and longer-term predictions (>months), particularly probabilistic forecasts are challenging using this modelling type and predicting beach recovery, which proceeds over timescales of years has also proved challenging, (Hanson et al., 2003).

In the last two decades several reduced complexity, equilibrium models have shown great potential in predicting shoreline change (e.g. Yates et al., 2009; Davidson and Turner, 2009; Davidson et al., 2013; Turki et al., 2013; Vitousek et al., 2017;). Unlike the detailed and computationally intensive physics-based models, these reduced-complexity, equilibrium models are stable, computationally efficient and permit fast probabilistic forecasts of coastal evolution, (Davidson et al., 2017). However, in spite of their proven potential to provide skilful long-term predictions of coastal evolution, equilibrium models frequently lack generality, requiring recalibration with extensive field data sets when transporting models from site-to-site. In this contribution, we explore the middle-ground between the process-based models and reduced complexity models and aim to develop a more versatile and physics-based equilibrium model, including the consideration of the specific morphological initial conditions and changing sea level.

Several dynamic-equilibrium models can be represented in the following generalised form:

$$\frac{d\zeta}{dt} = \mu\mathcal{F}[\psi_e - \psi] \quad (1)$$

In the above, the term on the left-hand side usually represents the temporal change in some aspect of the nearshore system. Examples include: shoreline displacement (Yates et al., 2009; Davidson et al., 2013), intertidal beach volume (Burvingt et al., 2018), sandbar position (Plant et al., 1999) and three dimensionality (Stokes et al., 2015), and even sediment grainsize (Prodger et al., 2016). μ is a response rate parameter, which is sometimes assigned different values for erosion and accretion, in recognition that these processes proceed at different rates and are controlled by different processes, (Splinter et al., 2014). The magnitude of shoreline change is generally related to the forcing $\mathcal{F}$, typically defined as

either incident wave power (P) or energy (E), depending on the author. The sign of the change is governed by the last (disequilibrium) term on the right-hand side of the equation. The definition of ψ varies from model to model but typically relates to the shoreline location (Miller and Dean, 2004), dimensionless fall velocity (Davidson and Turner, 2009) or wave energy (Yates et al., 2009/2011), again depending on the author. The disequilibrium-term is effectively the instantaneous perturbation of the controlling parameter (ψ) relative ψ_e. ψ_e is often (but not always) computed as the long-term mean, or sometimes weighted average antecedent value of ψ.

Yates et al., (2009/2011), defined $\mathcal{F}$ in equation 1 as the square root of wave energy ($E^{0.5}$), ψ $=E$ and ψ_e was not a long-term average in this instance, but instead, it is related linearly to the measured shoreline position x where:

$$\psi_e = ax + b. \quad (2)$$

Here a and b are empirical coefficients. This model also yielded good hindcasts with observations at two Pacific sites in the USA.

A similar model was proposed by Davidson et al., (2013) and Splinter et al., (2014), who found that setting $\mathcal{F}$ proportional to the square root of the incident wave power, ψ equal to the dimensional fall velocity and ψ_e equal to a weighted average of the antecedent values of ψ provided a skilful model for shoreline displacement at 8 very different sites around the world. In this model the magnitude of the shoreline displacement was logically related to the incident wave power and erosion followed if the instantaneous wave steepness exceeded the antecedent values, and visa-versa for accretion.

A recent review of the performance of several of the leading equilibrium and data learning shoreline models by Montaño et al., (2020), showed very similar model performance between a rage of different models, even given the differences in the model formulations.

In order to simplify mathematical developments later in this paper, it is useful at this point, to define some notation for a disequilibrium operator ($\widehat{\ }$), whereby:

$$\widehat{\psi}(t,\phi) = \psi_e(t,\phi) - \psi(t) \quad (3)$$

In the above, ψ represents any parameter, the angular overbar is the disequilibrium operator and ψ_e is the average (or optionally the weighted average) of the antecedent values of the same variable over the time interval ϕ. Splinter et al., (2014) found that the antecedent averaging window duration was a function of surfzone width (or beach-type), whereby dissipative beaches were more seasonally dominated, requiring longer averaging periods, compared to their reflective counterparts, which were more storm-dominated. It was hypothesised by Davidson et al., (2017) that this divergence in averaging-time related to the efficiency of transfer of sediment between the surfzone and offshore region. Unlike the one-dimensional pre-cursers, the present model negates the need for a variable averaging time, by explicitly modelling sediment-transport across the surfzone and offshore regions.

Inside the surfzone both process modellers (c.f. Aarninkhof et al., 1998 & Roelvink et al., 1995) and theoretical developments (Dean, 1977; Kriebel and Dean, 1985; Larson and Kraus,

1989) have recognised the link between wave energy dissipation and sediment transport. Outside the surfzone, in the absence of wave breaking, it has been observed that the sediment flux is functionally depended on the disequilibrium in the sea-bed slope, wave energy and water depth (e.g. Masetti et al., 2008; Patterson and Nielsen, 2016). Patterson and Nielsen, (2016) noted that local disequilibrium in profile gradient on the Gold Coast, resulting due to a relic river deposit, drove onshore transport. The magnitude of the slope-driven transport was proportionate to the wave energy and the disequilibrium in the profile gradient, and inversely proportional water depth. The present model developments encapsulate these observation, expressing the total sediment transport as the sum of wave dissipation and slope-driven components. Here there are also strong parallels between the SBEACH model (Larson and Kraus, 1989) and the ForCE model presented here. Both models contain dissipation and slope-driven components in the surfzone. However, it will be seen that the specific parameterisation and spatial extent of these parameterisations differ greatly.

Generally, the application of reduced complexity models on coastlines with significant longshore transport have involved combining cross-shore disequilibrium models with traditional one-line models (e.g. Robinet et al., 2018; Vitousek et al., 2017). Here, we use the term ‘one-line model’ to indicate a model that predicts shoreline evolution in response to strong longshore gradients in sediment transport. However, disequilibrium concepts have also been applied directly in models designed to predict the shoreline evolution due to longshore sediment transport. Turki et al., (2013) for example, presented a model for beach rotation driven by the incident wave energy flux and disequilibrium between the instantaneous and equilibrium shoreline orientation. In the present paper, we focus on cross-shore transport prosses and longshore uniformity is assumed, although the potential coupling with other models that predict longshore sediment transport is explored briefly in section 2.

This paper begins by describing the theoretical basis of the new model (section 2). There is a description of the field site and data used to test the model in section 3. In section 4 (results) the model is calibrated and validation using field data and a sensitivity analysis of the model to free parameters is conducted. A discussion and concluding remarks are given in sections 5 and 6 respectively.

2. Model Development

This section describes the development of a model for Forecasting Coastal Evolution (ForCE). Here equations for a 1-D, depth-average coastal profile model are derived. This computationally efficient model, permits long model runs and easy comparison with field data. It is noted that the same approach is theoretically possible for a one-line (shoreline model), or a 2-D area model, but neither of these are explored in the present paper.

The ForCE model links sediment transport directly to wave energy dissipation, without the intermediate step of computing surfzone currents. Two mechanisms for forcing sediment transport are recognised here. The first generates a perturbation from equilibrium (or disequilibrium), and has a magnitude and direction given by the disequilibrium in the turbulent-dissipation, due to wave breaking. The second transport term, acts to restore

equilibrium and is proportional to the local disequilibrium in bed-slope. Physically, this second term represents the natural balance between the processes that drive net sediment transport, including the undertow, wave asymmetry and gravitational forces. The concept here is that as the dissipation of incident waves change, relative to antecedent average conditions, then the balance between offshore and onshore sediment transport processes is perturbed and the beach flattens or steepens, by moving sediment out of, or into the surfzone respectively. Working against this perturbation is a diffusive restoring force, which acts to maintain the equilibrium-profile. The combination of these two forces is not entirely independent and results in a dynamic equilibrium.

In the following section model developments are based on a coordinate system whereby the *x*-axis increases positively shoreward. The vertical dimension (*z*) is measured relative to the mean water level, (Figure 1).

The ForCE model assumes that the instantaneous beach profile *z*(*x*, *t*), can be decomposed into a disequilibrium or fluctuating component $\hat{z}$ and a static or slowly changing dynamic-equilibrium profile z_e, such that:

$$z(x,t) = z_e(x) + \hat{z}(x,t) + \widehat{z_e}(x,t) \quad (4)$$

In a steady state system, it can be assumed that temporal variation in the equilibrium profile $\widehat{z_e} \approx 0$. However, long-term changes in environmental variables pertaining to sea level or wave climate for example, can lead to a dynamic equilibrium and slow temporal variability in z_e.

In this section, a sediment transport equation is derived, using a simple energy balance approach, whereby the available energy for sediment transport by wave dissipation, is balanced with the theoretical work done required to move a fixed volume of sediment. This new sediment transport equation is then combined with equilibrium considerations to derive an expression for the sediment transport associated with the beach perturbation $\hat{z}$, hereafter referred to as the ***'perturbation transport'***. The methodology for computing the equilibrium dissipation and beach profiles (z_e) is then described. Finally, the computation of the dynamic equilibrium component ($\widehat{z_e}$) is discussed in section 2.8.

2.1. Hydrodynamics

The ForCE model explicitly includes both changes in wave energy dissipation and sea level at every model time-step (typically = 1 hour). It is possible to increase (or reduce) this time-step, whilst preserving model stability. However, the maximum run-up and hence shore-face and dune erosion predictions would be significantly aliased by increasing the model time-step. This would also affect the fidelity of short term (e.g. storm erosion) model predictions and their subsequent impacts on longer term coastal erosion.

The energy balance which yields a solution to the spatial evolution of wave height is given by:

$$\frac{\partial P}{\partial x} + D_w + D_f = 0 \quad (5)$$

Where, D_w and D_f are the wave energy dissipation due to wave breaking and bed friction respectively. The temporal variation in sea level measured vertically upwards from the still water level is modelled as:

$$\eta = \eta_{tide} + \eta_{surge} + \eta_{setup} + \eta_{SLR} \quad (6)$$

The terms on the r.h.s. of this equation are the tide, surge, wave set-up and sea level rise components respectively. And the total water depth *h* measured positively downwards from the instantaneous water surface is given by:

$$h = \eta - z \quad (7)$$

where the still water level reference is at z = 0 m and the seabed is elevation is z.

The wave setup is modelled conventionally based on cross-shore gradients in radiation stress $\left(S_{xx} = \left(\frac{1}{2} + \frac{2kh}{\sinh(2kh)}\right) E_x\right)$, where the wave energy is $E_x = \rho g H_{rms}^2 \cos(\alpha)/8$ and α is the incident local wave angle derived from Snell's law. The wave set-up (η_{setup}) is extracted from solution of the following momentum balance:

$$\frac{dS_{xx}}{dx} + \rho g h \frac{d\eta_{setup}}{dx} = 0 \quad (8)$$

In the above H_{rms} is the local r.m.s. wave height, ρ is the density of water, k is the wavenumber and g is the acceleration due to gravity.

2.2. Wave dissipation-driven sediment transport

Consider a fixed volume of sediment (*V*) that is to be moved horizontally a distance x. The work done (W) in this horizontal translation is a product of the immersed weight of sediment and the distance moved:

$$W = (\rho_s - \rho) a\, V\, g\, x \quad \text{[J]} \quad (9)$$

Here, ρ_s is the sediment density, *a* is (1 – sediment porosity) and *V* is the sediment volume transported (per meter coast).

Differentiating equation 4 with respect to time and horizontal distance gives the following equation for gross sediment transport:

$$q_g \propto \frac{1}{(\rho_s - \rho) a g} \left(D_w + D_f\right) \quad [\text{m}^2/\text{s}] \quad (10)$$

Here, $q_g = \frac{\partial V}{\partial t}$ is the total gross sediment flux and $-\left(D_w + D_f\right) = \frac{\partial P}{\partial x}$ is the total wave power dissipation required to move the volume of sediment, through either turbulence induced by wave breaking D_w, or dissipation due to bed friction D_f associated with wave orbital velocities at the seabed. Thus, two separate sediment transport components can be identified in equation 10, which will be further expanded on the following sections in terms of their contribution to perturbation sediment transport.

2.3. Perturbation sediment transport due to turbulent wave dissipation (D_w)

Wave shoaling and dissipation are modelled using a Battjes and Janssen, (1978) wave energy dissipation model. This model computes D_w as a function of the local root-mean-square wave height, peak wave period T_p and probability of wave breaking, Q_b, where:

$$D_w = \frac{\alpha \rho g H_{rms}^2}{4\, T_p} Q_b \quad (11)$$

And,

$$\frac{1-Q_b}{\ln(Q_b)} = -\left(\frac{kH_{rms}}{0.28\,\pi\, tanh(kh)}\right)^2 \quad (12)$$

The turbulent dissipation due to wave breaking at the seabed, allowing for the decay with depth, is estimated by:

$$D_w \rightarrow f_w D_w \quad \text{[W/m]} \quad (13)$$

Where, f_w is function describing the decay of wave generated turbulent kinetic energy with depth. Following previous observations that turbulence induced by wave breaking decays exponentially with depth (c.f. Babanin, 2006), this is parameterised as follows:

$$f_w = exp\left(-\frac{\pi h}{H_b}\right) \quad (14)$$

Here H_b is the instantaneous wave breaker height. Notice that the effective impact of wave dissipation becomes negligible at the approximate depth of closure ($\approx 2H_b$).

It assumed here that the perturbation sediment transport due turbulent dissipation of incident waves is due to the disequilibrium in the dissipation $\widehat{D}_w$, therefore the first term in equation 10 becomes:

$$q_w = \frac{k_1}{(\rho_s-\rho)ag}\widehat{D}_w \quad (15)$$

Here, k_1 is a model calibration parameter, analogous to an efficiency term, representing the fraction of the dissipated wave power that contributes directly to moving sediment. The remaining power fraction (1-k_1) goes into moving water, sound, heat and other sources. In practical terms, k_1 is a response rate parameter that acts a linear scale factor for the morphodynamic response.

2.4. Slope-driven transport forced by bed dissipation (D_f)

Several authors (e.g. Larson et al., 1999; Masetti et al., 2008; Patterson and Nielsen, 2016; Steetzel, 1995) have reported a slope-driven transport towards equilibrium proportional to the disequilibrium in the beach gradient ($q \propto \left(1-\frac{\beta}{\beta_e}\right)$ or $\hat{\beta} = \frac{d\hat{z}}{dx}$) and the incident wave energy. Incident waves are responsible for mobilising sediment through local wave-energy dissipation and the action of wave orbital velocities at the sea-bed. Here β_e is the equilibrium seabed gradient. It has also been observed that although this transport component is inversely related to the water depth, it can still dominate outside the surfzone in the absence of wave-driven radiation stresses, (Patterson and Nielsen, 2016).

A beach gradient disequilibrium sediment transport term is also included in the ForCE model, which satisfies these observations. This transport component is a key driver of beach recovery and is instrumental in moving sediment deposited outside the surfzone during storms back to the intertidal surfzone region. Here the slope-driven transport is parameterised as:

$$q_s = q_o \frac{\widehat{\beta}}{\bar{\beta}_e} \quad \text{[m}^3\text{/s/ m wavelength]} \quad (16)$$

$\bar{\beta}_e$ is the spatial-mean gradient of the equilibrium profile for the region bounded by the depth of closure to the landward limit of the swash zone. Notice that, under-steepness (negative $\hat{\beta}$) conditions (i.e. local beach gradient < local equilibrium profile gradient), leads to onshore sediment transport and visa-versa.

The parameterisation of q_o in equation 16, is the subject of ongoing investigation, but the following dimensionally correct parameterisation follows from equation 10, which links the slope-driven transport to the wave energy dissipation due to friction and is consistent with the observations that slope-driven transport decreases with depth and increase with incident wave energy:

$$q_o = \left[\frac{k_2}{(\rho_s-\rho)ag}\right] D_f \quad (17)$$

Here k_2 is a second dimensionless model free parameter and the dissipation due to bed friction is given by:

$$D_f = \frac{\rho f}{12\pi}\left(\frac{\pi H_{rms}}{T_p sinh(kh)}\right)^3 \quad (18)$$

Here, f is a friction factor (Van Rijn, 1993), defined as:

$$f = exp\left(-6 + 5.2\left(\frac{2\sinh kh}{0.025H_{rms}}\right)^{-0.19}\right) \quad (19)$$

2.5. Total transport

The total perturbation transport is given by the linear sum of sediment transport components:

$$q = q_w + q_s + q_{ss} \quad (20)$$

The first two terms in equation (20) are somewhat analogous to the traditional sediment transport models that express total load transport as the linear sum of suspended and bedload components. However, instead of differentiating transport components in terms of the mode of sediment transport (i.e. suspended and bedload), here it is partitioned in terms of the forcing mechanism (i.e. dissipation due to wave breaking dissipation and slope-driven transport). The third term on the right-hand side of equation 20 (q_{ss}), accounts for the sum of any external sources or sinks of sediment, which must be either known quantities, (e.g. a beach replenishment scheme) or specified by and external model. q_{ss} is specified as a time-series and the cross-shore distribution is assumed constant between the depth of closure and berm height, although other parameterisations for the cross-shore variation can easily be imposed. This latter term makes coupling of the ForCE model with a one-line model possible, thus potentially allowing the impacts of gradients in longshore sediment transport to be accounted for, although this is beyond the scope of the present paper.

2.6. Bed evolution equation, ($\hat{z}$)

Assuming that sediment source/sink contributions are negligible, equation 20 can be recast into a bed evolution equation through application of the continuity equation.

$$\frac{\partial \hat{z}}{\partial t} = \frac{dq_w}{dx} + \frac{dq_s}{dx} \quad (21)$$

$$\frac{\partial \hat{z}}{\partial t} = c_1 \frac{\partial \hat{D}_w}{\partial x} + \frac{c_2}{\bar{\beta}_e}\frac{\partial}{\partial x} D_f \frac{\partial \hat{z}}{\partial x} \quad (22)$$

Here, $c_1 = k_1 c$, $c_2 = k_2 c$ and $c = [(\rho_s - \rho)ag]^{-1}$, $\hat{\beta}\left(= \frac{d\hat{z}}{dx}\right)$ is the beach gradient disequilibrium.

The first term on the r.h.s. of equation 22 describes the perturbation from the equilibrium profile as a function of the cross-shore gradient in the dissipation-disequilibrium. The second term is a diffusion term, which dissipates this perturbation in time and space. Functionally, this second term acts to smooth and dissipate any perturbations in the profile generated by the first term. Thus, increasing the diffusion constant k_2 effectively damps sand-bar formation and acts to restore equilibrium, enhancing the post-storm recovery of the intertidal beach. It is noted that terms one and two are not independent from one another, but will interact non-linearly. Nonetheless, equation 22 is an attractive formulation for a profile model as it has numerically efficient and stable numerical solutions, permitting long-term simulations. The first term on the r.h.s. of equation is solved explicitly in a second order Forward Time Backward Space finite-difference scheme and the second term is solved semi-implicitly using a flux conservative Crank-Nicholson solution.

2.7. Model spin-up: Derivation of the equilibrium bed level z_e and dissipation maps D_e

Unlike many other profile models (e.g. Larson and Kraus, 1989) the equilibrium bathymetry and dissipation maps are not assumed to be known *a priori*, or defined by pre-set mathematical functions. Instead, the approach taken here will be to compute these iteratively during a model spin-up period, initiated with a known initial and beach profile. The advantage of this methodology is that the resulting base equilibrium profile z_e, is likely a closer match to the observed profile than an alternative mathematical fit.

The idea of the model spin-up phase is to remove the imprint of the initial beach profile and replace it with a smoother '*equilibrium*' profile and associated dissipation map that is a reasonable representation of their annual average values. Thus, we require that the averaging period ϕ, is an integer number of years in order to obtain a reasonable estimate. D_e is the long-term temporal integration of the instantaneous dissipation due to wave breaking for all wave and tidal conditions (Figure 1).

$$D_e = \int_0^{\phi} D(t,x)dt \quad (23)$$

Here the initial conditions for D_e are derived by running the wave dissipation model over a fixed initial measured bathymetry for a model spin-up period of ϕ years. The mean equilibrium bathymetry is then computed, based on a temporal average of the modelled bathymetry over the same ϕ-year period,

$$z_e = \int_0^{\phi} z(t,x)dt \quad (24)$$

and finally, D_e is re-calculated using this equilibrium bathymetry. Note that the model spin-up requires only wave and water level data, plus an initial bathymetry. Waves and tidal elevation are normally quite readily available from either model output or direct measurements, so this is not considered to be a significant limitation of the model. Experimentation showed that the model sensitivity (in terms of modelled profile change) to ϕ is negligible in terms of model predictions for $\phi \geq 5$ years, so this value was selected for all tests presented in section 4.

Although the accuracy of this method for computing the base equilibrium profile remains to be tested against field observations, it is anticipated that this methodology will likely be an improvement on the theoretical beach profile fits to the observations that are frequently applied to profile models.

2.8 Derivation of $\hat{z}_e$: Model adaption to changing sea level

Over, time-scales of less than a decade, it may be reasonable to assume that the underlying equilibrium profile is constant and that temporal fluctuations about this equilibrium are adequately modelled by $\hat{z}$. However, over the longer term ($\gtrsim$10 years), it is a fundamental requirement of the model, to be able to adapt to changing environmental conditions, including changing sea level.

Here, a novel approach is adopted to computing the perturbation of the equilibrium profile. The methodology computes the optimal sediment transport (or minimum transport cost) to a new equilibrium state, resulting from sea level change. The method is based on minimising the transport cost and involves finding a solution to the Poisson equation for known restraints on boundary conditions.

The basic premise of the sea level adaption model implemented here is not new though (c.f. McCarroll et al., 2021) and is as follow: During sea level change, the ForCE model perturbs the equilibrium profile according to two conditions:

Condition 1: The shape of the equilibrium profile in the active transport zone between the depth of closure and berm height is conserved and elevated by η_{SLR}.

Condition 2: Sediment volume is conserved.

Condition 1 is considered to be a reasonable assumption, providing the sediment characteristics and wave climate are reasonably consistent in time, noting that changes in the total profile (z) in response to a non-stationary wave climate will be generated through $\hat{z}$.

Mathematically, condition 1 can be expressed as:

$$\hat{z}_e(t,x) = z_e^n(x-\tau) + \Delta\eta_{SLR} - z_e^{n-1}(x) \quad (25)$$

Here $z_e^{n-1}(x)$ represents the equilibrium profile prior to an incremental sea level rise $\Delta\eta_{SLR}$ and z_e^n is subsequent profile elevation, which is also subject to an unknown horizonal translation τ in the *x*-direction. Equation 25 is only finite for the domain extending offshore as far as the depth of closure ($x > x_{DOC}$) and inshore as far the run-up limit ($x < x_{Berm}$), allowing for the horizontal translation (τ). Note that the assumption is made here that the profile response to sea level rise is instantaneous. This simplifying assumption is deemed to be sound as calculations of the average morphodynamic response rates are at least an order of magnitude higher than the rate of sea level rise.

Equation 25 is solved iteratively for the value of τ that closes the sediment budget (condition 2), whilst simultaneously minimising the transport-cost. To achieve this ForCE implements a method outlined in Bosboom et al., (2020), originally postulated as an improved

methodology for assessing the skill of morphodynamic models. Here the potential (χ) is defined, which is related to the equilibrium profile perturbation ($\hat{z}_e$) by:

$$\nabla^2\chi = \hat{z}_e \quad (26)$$

Optimum sediment volume transport (m^3/m coast) to equilibrium (V_e) is found via integration of the Poisson equation (22) w.r.t. *x*:

$$V_e = \nabla\chi, \quad (27)$$

The Poisson equation is irrotational and yields a unique solution for χ and hence V_e, if the boundary conditions are known. Here, no prior assumptions are made regarding either boundary being closed, and both the offshore and shoreline boundaries are specified as open (Dirichlet), such that sediment transport-cost towards equilibrium is minimised. Note that this requires no *a priory* assumption regarding a closed (Neumann) boundary at either the depth of closure, or the shoreline. Under some circumstances a solution might be sought for a zero sediment-flux boundary if this is known with certainty and this can be controlled by the user. An obvious example is where there is a sea wall at the landward boundary.

The law of sediment conservation requires that the sediment gain or loss over the whole profile is zero. The Poisson equation is solved iteratively for different τ-values until this condition is satisfied, i.e.

$$V_0 + V_c \rightarrow 0 \quad (28)$$

Where, V_0 and V_c are the boundary values for sediment volume change (V_e) at the shoreline and depth of closure respectively.

The Poisson equation is solved numerically using a the same semi-implicit, Crank-Nicholson finite difference scheme as equation 22. As sea level rise proceeds at a rate of mm/year, a solution for $\hat{z}_e$ is not required every model time-step and can be limited to times when sea level change exceeds a user-defined threshold value, allowing considerable gains in computational efficiency. Once a solution for τ is obtained, then the equilibrium dissipation map D_e is spatially translated by the same amount avoiding computationally intensive recalculation.

2.9. Swash zone sediment transport

A fairly simplistic treatment of the swash zone is adopted here, by extending the equilibrium profile z_e, computed during spin-up, landward, via a simple linear extrapolation beyond the mean high-tide elevation (figure 1). This linear extrapolation is required as this region of the beach is less frequently subject to surfzone processes and therefore a reliable value for the equilibrium beach is not necessarily obtained during spin-up, particularly at the shoreward limits of extreme run-up. The instantaneous 2% run-up exceedance limit due to wave setup and swash, included is computed via the Stockdon et al., (2006) equation.

$$\eta_{R2\%} = 1.1(0.35tan\beta(H_0L_0)^{0.5} + 0.5[H_0L_0(0.563tan^2\beta + 0.004))]^{0.5}) \quad (29)$$

Here the subscript 'o' denotes deep water values and *L* is the wavelength. Note that the first term on the right-hand side of equation 29 is an empirical prediction of wave setup, which is used in place of the value obtained from equation 8 for the calculation of the shoreward limit of the surfzone.

3. Field site

Perranporth is a 3.5 km long, macrotidal beach (mean spring range = 6.5 m) situated on the north Cornwall coastline in the UK (Davidson et al., 1997, Figure 2 & 3). It is fully exposed to energetic Atlantic swell, with mean significant wave height and peak period equal to 1.56 m and 10.5 s respectively. The site is dominated by shore-normal waves and cross-shore sediment transport processes, which explain >80% of the total sediment transport at this site (Burvingt et al., 2018), making it an ideal site for application of this profile model.

The beach sediments are quartz sands, with a median grainsize of ≈ 0.33 mm. The wave climate is highly seasonal, with larger wave periods and heights characterising the winter months (Figure 3). The beach morphology varies through the year and can typically be classified as dissipative (dimensionless fall velocity > 5) in the northern hemisphere winter to low-tide bar and rip in the summer (dimensionless fall velocity <5), (Masselink and Short, 1993).

3.1. Typical morphodynamic response

Based on annual bathymetries and monthly inter tidal surveys recorded over a 10-year period and hourly recorded time-averaged video images initiated in 1991, the following qualitative seasonal evolution patterns are observed.

During the winter period (November-February) the dissipative beach classification is synonymous with rapid intertidal erosion and the deposition of offshore sand bars. The erosional-bars, are typically located seaward of the low water contour, their precise location is dependent on the size of the incident waves and width of the surfzone. The extreme storm bars can be located far from the shore and contain large volumes of the total beach sand budget and are often observed $\approx 0.7 - 0.8\ km$ seaward of the dune foot, (Valiente et al., 2019). Pertinent to the model predictions in the next section, this offshore bar is persistent in time, varying in volume and location, but forming a semi-permanent feature.

During the much longer slower recovery period (typically March to October), sediment is returned from offshore bar(s) to form accretion-bars on the lower (most seaward) intertidal zone. As recovery progresses under smaller wave conditions, the sand deposited initially in the lower-intertidal region migrates shoreward, replenishing the intertidal profile and causes a progradation of the high-water shoreline contour. The cross-shore sediment transport process described above shows a ‘cut-and-fill’ process (Komar, 1976), with a nodal location approximately around the lower-tide shoreline location (c.f. Valiente et al., 2019).

3.2. Model forcing and initial conditions

In the following section, the model is forced using modelled wave data from the Met Office Wave Watch III model for a grid-point located in 17m water depth (Lat: 50.35279, Lon: -5.17424), directly offshore of the modelled profile location (figure 3). The model is also forced with predicted tides from a harmonic tidal model, which has been calibrated with field observations from a local pressure transducer. Figure 3 shows a subset of the forcing time-

series recorded between 2000 and 2020. Notice the highly seasonal wave height and period and the advent of a major storm sequence in the 2013/14 winter period (Scott et al., 2016).

The model is initiated with a beach profile that is monitored biannually by Channel Coastal Observatory (CCO, https://www.channelcoast.org/) from 2008 until present day. A further high temporal resolution (monthly) survey programme is used to calibrate the model. This is randomly sampled (spatially), using a kinematic, differential GPS survey conducted by Plymouth University's Coastal Processes Research Group (CPRG, https://www.channelcoast.org/) using a quadbike and subsequently interpolated along the same CCO survey line (Unique ID: 7a01444). Although the different sampling methods and interpolation inevitably leads to some divergence between the CCO and CPRG surveys, the high temporal resolution of the CPRG survey provides a robust test of the model's temporal prediction of shoreline evolution and is ideal for model calibration, whilst the repeat profile surveying approach adopted by the CCO makes an ideal data set for spatial comparisons between modelled and measured beach profiles. Therefore, both surveys are used here to validate the model.

The biannual CCO intertidal beach surveys, between 2008 and 2019 are averaged in time and used to initialise the ForCE model, noting that the model can be run with a single initial profile. Calibration and validation of the model is achieved with the monthly resolved CPRG surveys, with full details of this process given in the next section. Figure 4 (upper panel) shows the limits of both the CPRG and CCO surveys. Notice the x-axis is equal to the negative of the CCO recorded chainage, as the model coordinate system must increase positively shoreward. The lower panel in Figure 4 shows the time variability of the +2m (rel. Ordinance Datum Newlyn) contour (approximately mean high water). Both the CPRG and CCO survey data are plotted here showing clearly the difference in temporal resolution. Whilst the two data-sets are highly coherent, there is some deviation, which can be explained by the different sampling strategies and the data interpolation. The CCO measurements can be considered to be the most accurate for representation of the modelled profile line and shoreline position, as they are measured on the profile line and not prone to errors introduced by longshore non-uniformities and interpolation. Therefore the r.m.s. differences between two surveys can be used to estimate the potential error bars for the CPRG shoreline time-series, giving a value of 4.27 m.

Notice that the shoreline time-series shows a clear seasonal variability, superimposed on strong interannual fluctuations. The extreme storm erosion in the winter of 2013/14 is also clearly evident here.

4. Results

In this section the ForCE model is compared qualitatively and quantitatively to a comprehensive data set described above. The aim here is to calibrate the model by assessing appropriate values of k_1 and k_2 with observations and to test the skill of the model against unseen data.

4.1. Model calibration, validation and skills scores

A simple calibration of the model is adopted here which is very quick and straight forward. Although, there is scope to improve this calibration process, using Kalman filters for example, this simple approach proved very effective. The model free parameters are optimised via an iterative least-squares comparison between the measured and modelled shoreline contour time-series (rather than whole profile comparisons). Here we select a contour at z = 2 m, which is approximately at the mean high-water level. First, k_2 is fixed, then k_1 is optimised through the least-squares comparison between modelled and observed shoreline predictions. The gradient-term in the regression between modelled and measured shoreline time-series provides a calibration multiplier for k_1, yielding an optimal value. The first five years of the dataset (2008-2013) are used for model calibration and the latter seven years (2013-2020) are left unseen in order to provide an unbiassed validation of the model performance. During the sensitivity analysis, k_2 is then adjusted to a new value and the processes is iterated.

The overall model skill for the full dataset including seen and unseen data, is assessed by simultaneously maximising the Pearson correlation coefficient (r) and minimising the normalised-mean-square error (NMSE) between the measured and modelled shoreline time-series in a combined skills score (CSS) computed as follows:

$$NMSE = \frac{1}{\sigma_m}\sqrt{\frac{1}{N}\sum_1^N\left(x_m - x_p\right)} \tag{30}$$

$$CSS = \frac{r_c^2 + r_v^2}{NMSE_c + NMSE_v} \tag{31}$$

In the above the σ represents the standard deviation, the subscripts m, p, c and v represent, measured, predicted (modelled), calibration and validation respectively. The full results of this analysis are summarised in table 1 and will be discussed later. The CSS parameter is designed to simultaneously maximise the coherence and minimise the deviation between the modelled and measured profiles.

4.2. Hydrodynamics & sediment fluxes

Figure 5 shows an example output for a typical wave condition from the model's hydrodynamic module. The upper plot shows the initial model beach profile and still water level. The middle panel shows the shoaling and dissipation of random waves and the evolution of wave set-up over the profile. The lower panel shows the computation of dissipation due to wave breaking and friction at the sea bed, which are of fundamental importance in the ForCE model.

The upper panel of figure 6 shows equilibrium dissipation map (D_e) for the beach profile, computed by integration of D_w over all tide and wave condition for a period of ϕ = 5 years with a time-step of 1 hour. Also shown (figure 6, upper panel) is the instantaneous breaking wave dissipation (D_w) for a mild storm event (H_s = 3 m, T_p = 10 s). For most of the surfzone $D_w > D_e$, leading to offshore sediment transport. Outside the surfzone, $D_w < D_e$, leading to onshore transport. The corresponding sediment flux computed using equation 15 is shown in

the middle panel of figure 6. The similarity of this flux pattern to the some field observations is striking (c.f. Mariño-Tapia et al., 2007). The corresponding bed-evolution due the wave dissipation component of sediment transport (q_w) is shown in the lower panel of figure 6. Here we can see strong erosion in the surfzone, milder erosion in the wave shoaling zone and accretion of bar located just seaward of the surfzone; a classic breakpoint bar. Note that this feature is emergent rather than being defined *a priori* by a sediment transport shape-function.

Figure 7, shows an equivalent plot for a low-wave condition (H_s = 0.5 m, T_p = 10 s). In this example, $D_w < D_e$ across the entire profile, leading to onshore transport (figure 7, middle panel). Divergence of the sediment transport leads to erosion in the region that the small waves are shoaling and accretion in the narrow surf-zone. Note that these instantaneous dissipation maps and flux profiles and bed responses are re-calculated with the tidal displacement, as the model steps forward in time.

4.3. Model calibration, validation and sensitivity analysis

The model calibration-validation process is illustrated in figure 8, which shows the cross-shore displacement of the 2 m contour line for both the CPRG measured shoreline position and the modelled equivalent. Here, Δx_s is the negative of the shoreline change in the model frame of reference, giving erosion as negative response. The gradient of the linear regression analysis between the 'seen' shoreline measurements and the model equivalents gives a multiplication factor used to adjust k_1, yielding an optimised value. This optimised value for k_1 is subsequently applied throughout the calibration and validation comparisons.

4.3.1. The recovery parameter, k_2

Figure 8 illustrates the impact on shoreline estimates caused by varying the model diffusion coefficient (or recovery parameter) k_2 from 0.005-0.04. Focussing on the validation part of the time-series (open squares) in figure 7, it can be seen the best model validation results occur for k_2=0.01. For this example, both the seasonality and interannual shoreline change is well predicted, as is the long-term multi-year shoreline recovery after the 2013/14 storms.

For k_2=0.005 (upper panel, figure 8), the modelled shoreline fails to recover adequately after the severe storm erosion in 2013/14. Conversely, for k_2=0.04 the shoreline over-recovers. It can also be seen that increasing k_2 has the impact of reducing the interannual variability in the modelled time-series.

The complementary modelled profile change ($\hat{z}$) for k_2 = 0.005, 0.01 and 0.04 is shown in figure 9. Encouragingly, these results show many of the observed morphodynamic features described section 3. Focussing first on the best validation from the shoreline analysis (k_2 = 0.01, middle panel, Figure 9), there is extreme erosion of the intertidal area during the 2013/14 storm sequence and addition of sediment to a persistent storm-bar ≈1 km seaward of the high-tide shoreline. This compares well with bathymetric analysis at Perranporth by Valiente et al., (2019) and observations from an Argus video station. This storm bar is persistent in time for k_2 = 0.01. The bar migrates offshore slowly due to non-linear feedback between the profile and hydrodynamics. Specifically, the formation of the bar causes waves

to break further offshore. The convergence zone in the flux profile, shown in figure 6 is also displaced seaward, leading to offshore bar migration. The storm-bar is diminished during 2015, when the slope-driven sediment-transport term (equation 16) is responsible for an onshore sediment flux in the region of the storm-bar returning sediment to the intertidal zone and diminishing bar magnitude.

During beach recovery months (March to October), sediment is mined from a region seaward of the low tide contour line ($x < -1500\ m$) and deposited around the seaward limit of the intertidal zone ($x > -1500\ m$). Over the course of the recovery period this intertidal recovery bar migrates landward, recharging the intertidal profile and prograding the shoreline contour (figure 9, middle panel). Notice also the presence of a 'cut-and-fill' nodal position around the approximate low-tide position, also consistent with the observations Valiente et al., (2019).

The impact of setting k_2 too high is seen in the lower panel of figure 9 (k_2 = 0.04). The interannual variability is unrealistically diminished, the extreme storm erosion is under-predicted and the subsequent beach recovery is too rapid. Conversely, setting k_2 too low (upper panel, figure 9, k_2 = 0.005) leads to an under-prediction of the beach recovery.

4.3.2. Modelled and measured profile comparisons

A direct comparison of the observed (CCO) and predicted profile evolution is shown in figure 10. Here the middle panel is a contour plot of the measured biannual profile evolution in time, measured relative to the initial profile. The time-series exceeds 10 years in duration. Steady intertidal accretion persists in the period 2008 to 2013, followed by extreme storm erosion (2013/14) and a slow subsequent recovery to 2019. The same patterns are evident in the modelled data (figure 10 lower panel), although the response is a little smoother than the observations. The modelled and measured intertidal beach volume between z = -2 to 5 m are shown in the upper panel of Figure 10. These vertical limits are constrained by the vertical extent some of the surveys. Also shown is the error in these predictions relative to observed range. Similar to the shoreline predictions the intertidal beach volume estimates vary coherently (r = 0.87) with the observations with mean errors of 9.9 %. Encouragingly, there is little evidence that this error increases with the prediction time ΔT, even up to 10 years.

For a clearer comparison of the measured and modelled profiles, figure 11 provides extreme storm and long-range recovery examples. The upper panel shows the initial measured profile recorded on the 21st September 2013. Also shown, is the subsequent profile measured 161 days later after the extreme storm sequence, alongside the matching model prediction. The wide-spread erosion of the intertidal profile by up to 0.5 m is reasonably well predicted by the model. The evolution of the profile above z = 4 m is not well predicted, but this to be expected as this area is above spring HW and subject to anthropogenic and aeolian processes, which are not modelled by ForCE.

Figure 10 showed a steady recovery of the beach profile over the period 2009 to 2013. This is further illustrated in the lower panel of figure 11. Again, the intertidal profile recovery is reasonably predicted by the model, even over this extended period, (ΔT=1657 days).

4.4. Multidecadal model forecasts and dynamic equilibrium

Figure 12 shows the results of two long-term (110 years) ForCE model runs, the first with no sea level change and the second with 1 m of sea level rise over the time-interval 2000-2100. Wave model output has been used to force this model run until 2000, after which synthetic waves have been used based on the methodology outlined in Davidson et al., 2017. The wave statistical properties are assumed to be stationary, thus isolating the morphodynamic impact of sea level rise.

Figure 12a shows the initial and final beach profile predictions from the model, both with and without sea level rise. Note that whilst both model-runs show the formation of a persistent storm bar, generated in response to the extreme storm events, the dune erosion is far more prominent in the sea level rise example, as one might expect.

Figure 12b shows the temporal evolution of the 2m contour, again plus sea level rise and without sea level rise. The sea level rise is shown on the secondary vertical axis. Also shown are the bathtub projections of the same contour which assumes that morphology is unchanged from its initial form. A Bruun Rule (Bruun, 1988) prediction is also shown for comparison with the model estimates.

Note that both the model runs, with and without sea level rise show a prominent morphodynamic response to the 2013/14 storm sequence, generating the persistent offshore bar in figure 12a. Whilst neither model run recovers completely from this extreme event, the shoreline prediction without sea level rise, proceeds after 2014, without a significant temporal trend until the end of the record. With sea level rise included the shoreline contour erodes significantly more, finishing 60m landward of the example without sea level rise at the end of the simulation. It is interesting to note that after about 35-40 years of sea level rise the two time-series are non-overlapping, indicating that sea level rise impacts exceed the natural variability associated with wave forcing after this period.

Clearly, it is not possible to test fully the integrity of any of these predictions using field measurements. However, it is interesting to note that in the absence of the extreme storms the Bruun prediction provides a similar estimation of the rate of shoreline recession to ForCE. Whereas the simple bathtub projection suggests a much smaller shoreline recession, (by factor of 3). Thus, the differences between ForCE and the Bruun Rule result primarily due to the impact of short-term variability (e.g. storms) on the long-term evolution of the profile and a more explicit treatment of the supratidal morphology (e.g. dunes) and the resulting impact on the coastal sediment budget. There is minimal feedback from the translation of the beach profile due to sea level rise to the short-term sediment transport terms in the ForCE equation (22), as the active profile shape (from the berm height to depth of closure) is preserved and

the average dissipation map is translated a horizontal distance commensurate with the that of the equilibrium profile.

In some senses the ForCE predictions of shoreline evolution are similar to the COCOONED model formulated by Antolínez et al., (2019), which also modelled the impacts of short-term cross-shore and longshore sediment transport processes alongside the much longer-term sea level rise impacts. Although, COCOONED is a shoreline model with more schematic representation of the supratidal morphology. It is worth noting that the ForCE model will be sensitive to the precise morphology of the supra-tidal beach as erosion as the dune system will contributes sediment to the intertidal beach and ameliorate the rate of shoreline recession.

5. Discussion

5.1. Model free parameters

A new profile model for Forecasting Coastal Evolution, ForCE, is presented here, which relates sediment transport directly to wave energy dissipation, without any *a priory* definition of arbitrary sediment transport shape-functions or idealised mathematical descriptions of the equilibrium beach profile. Thus, any morphodynamic features which develop are truly emergent, rather than being pre-determined.

There are strong parallels between the SBEACH model (Larson and Kraus, 1989) and the ForCE model presented here. Both models are profile models that contain dissipation and slope-driven components in the surfzone. However, the specific parameterisation and their spatial extent differ greatly. SBEACH for example, computes the dissipation term as the disequilibrium between the instantaneous wave energy dissipation due to breaking and a predefined equilibrium value. The latter is functionally dependent on the sediment grain size and relates to a theoretical model of equilibrium beach profile, of the form $h=Ax^{2/3}$, (h=water depth, x=cross-shore distance, A=grain size dependent constant). In the present model the equilibrium reference dissipation is determined differently (see section 2) and unrelated to any pre-defined mathematical description of the equilibrium profile. Furthermore, SBEACH subdivides the beach profile spatially into four different regions, with an equivalent number of sediment transport equations. In SBEACH, the slope-driven and dissipation driven terms are only explicitly defined in the surfzone and attenuated exponentially beyond. By comparison the model developments in this contribution recognise a single sediment transport equation with only two empirical coefficients and both dissipation and slope-driven sediment transport components are explicitly defined over the whole profile.

The first transport term in ForCE acts to perturb the equilibrium profile and is a function of the disequilibrium in wave-breaking dissipation. Conversely, the second transport term acts as a restorative term, recovering equilibrium and is functionally dependent on the slope disequilibrium. There are two dimensionless free parameters associated with these sediment transport equations. The first k_1, is a response rate parameter controlling the perturbation component (q_w) and exerts a linear control on the magnitude of the morphodynamic response.

k_2, the recovery parameter, is associated with the restoring term (q_s) and controls the rate of post storm recovery in shoreline position and intertidal beach volume.

Table 1 summarises the model free parameter sensitivity analysis in terms of the Pearson correlation coefficient, the normalised mean-square-error and the combined skills score. Note that there is little variability in the optimised response rate parameter k_1, which remains $\approx$0.01 throughout, irrespective of the values selected for k_2. Thus, although the two terms in on the right-hand side of the bed evolution equation interact non-linearly, the magnitude of k_1 and k_2 do not seem to be strongly co-dependent.

The most skilful model predictions (highlighted in bold in table 1) in terms of the shoreline time-series comparisons, gives k_1=0.01 and k_2= k_1, which produce both skilful prediction of shoreline position and beach volume as well reproducing storm-bar dynamics which qualitatively match with observations. Application to a much wider range of field datasets will be required in order to assess the extent to which these parameters vary from site to site.

5.2. Spatial scales

Model results (e.g. figure 9) consistently predicted the occurrence and correct cross-shore location morphodynamic features. For example, the location of the nodal position in the beach change predictions $\hat{z}$ and the location of the offshore bar following the extreme 2013/14 storms all match observations (Valiente et al., 2019). The topographic-difference maps presented in Valiente et al., (2019), indicate that the nodal location was approximately 0.5-0.6 km from the dune foot and the storm bar was located 0.7-0.8 km from the dune foot after the 2023/14 storms. Inspection of Figure 9 shows that the dune foot is located at approximately x = -1000 m and that the distance from here to the nodal location and storm bar are approximately 0.5 km and 0.8-1 km respectively. Although these predictions and measurements are comparable, it is recognised that the cross-shore scale of these features will be sensitive to the pattern of wave-energy dissipation predicted by the hydrodynamic module. In this contribution the Battjes and Janssen, (1978) model was run with default parameters and no attempt was made to tune or optimise the cross-shore scaling of morphodynamic features, although it is expected that the location of the observed features will in reality be affected by the coefficient embedded in the wave dissipation model.

5.3. Planned future model developments

The simplicity, computational efficiency and stability of the ForCE model highlights the potential for multi-decadal predictions of coastal evolution and the potential for providing a coastal management tool for assessing coastal resilience in a changing climate of waves and sea level. The potential of the model to incorporate other sources and sinks of sediment, briefly described in the model description section, provides a theoretical basis for coupling the ForCE model with a longshore sediment transport model, the simplest of which would be a convectional one-line model. A new one-line shoreline model based on identical theoretical concepts described in section 2 is currently in development. The aim of this work is to couple the new one-line model with FoRCE in a quasi-2D area model. It is envisaged that the resulting simplicity of this genre of model will facilitate long range, multi-decadal

probabilistic forecasts of coastal evolution (e.g. Davidson et al., 2017), which can be applied to a broad range both cross-shore and longshore transport dominated coastal environments.

6. Concluding remarks

In the previous section a new coastal evolution model has been derived, calibrated and tested using field data. In this model, two sediment transport-components have been defined. The magnitude of these two transport-components are linked directly to magnitude of wave energy dissipation by wave-breaking and bed-slope disequilibrium respectively and negate the usual step of generating surfzone currents. The direction of the breaking-dissipation component is in the plane of wave propagation and has a sign equal to that of the disequilibrium in dissipation by wave breaking. The direction of the second component is determined by the local bed-slope disequilibrium and acts to restore equilibrium. Thus, the first dissipation term causes a perturbation in the profile, whilst the second term acts as a restoring force. Both transport components reduce exponentially with depth and are proportionate to the incident wave energy.

The Forecasting Coastal Evolution (ForCE) model equations have been derived for a depth averaged coastal profile model, assuming longshore uniformity in the beach profile and negligible gradients in longshore sediment transport. The resulting profile-model provides accurate long-term predications of shoreline position and the change in volume of the intertidal zone, over times scales spanning an individual storm, storm-sequences and multi-year beach recovery. Indeed, accurate predictions of shoreline position and beach volume were possible at this field site for time-scales of more than a decade with mean errors of less than 10%.

Emergent features like the formation and location of storm bars were qualitatively accurately predicted in response to the extreme storm sequence of 2013/14. The model was also able to reproduce other observations such as a beach-change minima (node), located just seaward of the low tide contour. The other morphodynamic process that was realistically reproduced was the process of beach recovery. During beach recovery (March-October), sediment was mined form seawards of the beach change node and deposited at the seaward limit of the intertidal zone. This accretion-bar feature then migrated landward, recharging the intertidal profile and prograding the high-tide contour. These morphodynamic predictions qualitatively matched observations and are emergent features that were not dependent on any predefined sediment transport or beach response shape function.

The encouraging field comparisons suggest that this model would have considerable practical application on cross-shore transport dominated coasts, potentially tracking morphological change between beach surveys and providing an early warning for coastal erosion and potential overtopping. The stability and efficiency of the model also promises potential application to Monte Carlo probabilistic forecasting of coastal evolution over much longer time-scales, (Davidson et al., 2017).

Acknowledgements

A special thanks to all members of Plymouth's Coastal Processes Research Group who contributed to the Perranporth data set included in this paper. The data collection at Perranporth was funded by NERC grants NE/M004996/1 (Urgency Grant) and NE/N015525/1 (Strategic Highlights Topic grant) and NE/N015894/1 (BLUE-coast). Thanks also to the Channel and Plymouth coastal observatories for the provision of their Perranporth survey dataset. Finally, thanks to Edward Steele and Andrew Saulter from the Met Office in the UK for the provision of the modelled wave data. I would also like to extend a sincere thank you to the reviewers of this paper who provided incredibly inciteful and helpful comments on the manuscript and have considerably improved this paper.

References

Aarninkhof, S., Hinton, C., Wijnberg, K., 1998. On the predictability of nearshore bar behaviour. Proc. Coast. Eng. Conf. 3, 2409–2422. https://doi.org/10.1061/9780784404119.181

Antolínez, J.A.A., Méndez, F.J., Anderson, D., Ruggiero, P., Kaminsky, G.M., 2019. Predicting Climate-Driven Coastlines With a Simple and Efficient Multiscale Model. J. Geophys. Res. Earth Surf. 124, 1596–1624. https://doi.org/10.1029/2018JF004790

Babanin, A. V, 2006. On a wave-induced turbulence and a wave-mixed upper ocean layer. Geophys. Res. Lett. 33, L20605. https://doi.org/10.1029/2006GL027308

Battjes, J.A., Janssen, J.P.F.M., 1978. Energy loss and set-up due to breaking of random waves. Proc. 16th Int. Conf. Coast. Eng. ASCE 569–587.

Bosboom, J., Mol, M., Reniers, A.J.H.M., Stive, M.J.F., de Valk, C.F., 2020. Optimal sediment transport for morphodynamic model validation. Coast. Eng. 158. https://doi.org/10.1016/j.coastaleng.2020.103662

Bruun, P., 1988. The Bruun rule of erosion by sea-level rise: a discussion on large-scale two- and three-dimensional usages. J. Coast. Res. 627–248.

Burvingt, O., Masselink, G., Scott, T., Davidson, M., Russell, P., 2018. Climate forcing of regionally-coherent extreme storm impact and recovery on embayed beaches. Mar. Geol. 401. https://doi.org/10.1016/j.margeo.2018.04.004

Davidson, M.A., Huntley, D.A., Holman, R.A., George, K., 1997. Evaluation of large scale (km) intertidal beach morphology on a macrotidal beach using video images, in: Coastal Dynamics - Proceedings of the International Conference. pp. 385–394.

Davidson, M.A., Splinter, K.D., Turner, I.L., 2013. A simple equilibrium model for predicting shoreline change. Coast. Eng. 73, 191–202. https://doi.org/10.1016/j.coastaleng.2012.11.002

Davidson, M.A., Turner, I.L., 2009. A behavioral template beach profile model for predicting seasonal to interannual shoreline evolution. J. Geophys. Res. 114, F01020. https://doi.org/10.1029/2007JF000888

Davidson, M.A., Turner, I.L., Splinter, K.D., Harley, M.D., 2017. Annual prediction of shoreline erosion and subsequent recovery. Coast. Eng. 130, 14–25. https://doi.org/10.1016/j.coastaleng.2017.09.008

Dean, R.G., 1977. Equilibrium beach profiles: U.S. Atlantic and Gulf Coasts, Ocean Engineering Technical Report, No.12, University of Delaware.

Hanson, H., Aarninkhof, S., Capobianco, M., Jime´nez, J.A., Larson, M., Nicholls, R.J., Plant, N.G., Southgate, H.N., Steetzel, H.J., Stive, M.J.F., Vriend, H.J. De, 2003. Modelling of coastal evolution on yearly to decadal time scales. J. Coast. Res. 19, 790–811.

Komar, P.D., 1976. Beach Processes and Sedimentation. Prentice Hall.

Kriebel, D.L., Dean, R.G., 1985. Numerical simulation of time-dependent beach and dune erosion. Coast. Eng. 9, 221–245. https://doi.org/10.1016/0378-3839(85)90009-2

Larson, M., Kraus, N.C., 1989. SBEACH: Numerical Model for Simulating Storm-Induced Beach Change - Report 1: Empirical Foundation and Model Development, Report CER. ed. U.S. Army Corps of Engineers.

Larson, M., Kraus, N.C., Wise, R.A., 1999. Equilibrium beach profiles under breaking and non-breaking waves. Coast. Eng. 36, 59–85.

Lesser, G.R., Roelvink, J.A., van Kester, J.A.T.M., Stelling, G.S., 2004. Development and validation of a three-dimensional morphological model. Coast. Eng. 51, 883–915. https://doi.org/10.1016/j.coastaleng.2004.07.014

Mariño-Tapia, I.J., Russell, P.E., O'Hare, T.J., Davidson, M.A., Huntley, D.A., 2007. Cross-shore sediment transport on natural beaches and its relation to sandbar migration patterns: 1. Field observations and derivation of a transport parameterization. J. Geophys. Res. 112, C03001. https://doi.org/10.1029/2005JC002893

Masetti, R., Fagherazzi, S., Montanari, A., 2008. Application of a barrier island translation model to the millennial-scale evolution of Sand Key, Florida. Cont. Shelf Res. 28, 1116–1126. https://doi.org/10.1016/j.csr.2008.02.021

Masselink, G., Short, A., 1993. The effect of tide range on beach morphodynamics and morphology: a conceptual beach model. J. Coast. Res. 9, 785–800.

McCarroll, R.J., Masselink, G., Valiente, N.G., Scott, T., Wiggins, M., Kirby, J.-A., Davidson, M., 2021. A rules-based shoreface translation and sediment budgeting tool for estimating coastal change: ShoreTrans. Mar. Geol. 106466. https://doi.org/10.1016/j.margeo.2021.106466

Miller, J.K., Dean, R.G., 2004. A simple new shoreline change model. Coast. Eng. 51, 531–556. https://doi.org/10.1016/j.coastaleng.2004.05.006

Montaño, J., Coco, G., Antolínez, J.A.A., Beuzen, T., Bryan, K.R., Cagigal, L., Castelle, B., Davidson, M.A., Goldstein, E.B., Ibaceta, R., Idier, D., Ludka, B.C., Masoud-Ansari, S., Méndez, F.J., Murray, A.B., Plant, N.G., Ratliff, K.M., Robinet, A., Rueda, A., Sénéchal, N., Simmons, J.A., Splinter, K.D., Stephens, S., Townend, I., Vitousek, S., Vos, K., 2020. Blind testing of shoreline evolution models. Sci. Rep. 10. https://doi.org/10.1038/s41598-020-59018-y

Patterson, D.C., Nielsen, P., 2016. Depth, bed slope and wave climate dependence of long term average sand transport across the lower shoreface. Coast. Eng. 117, 113–125. https://doi.org/10.1016/j.coastaleng.2016.07.007

Plant, N.G., Holman, R.A., Freilich, M.H., Birkemeier, W.A., 1999. A simple model for interannual sandbar behavior. J. Geophys. Res. Ocean. 104, 15755–15776. https://doi.org/10.1029/1999JC900112

Prodger, S., Russell, P., Davidson, M., Miles, J., Scott, T., 2016. Understanding and predicting the temporal variability of sediment grain size characteristics on high-energy

beaches. Mar. Geol. 376. https://doi.org/10.1016/j.margeo.2016.04.003
Robinet, A., Idier, D., Castelle, B., Marieu, V., 2018. A reduced-complexity shoreline change model combining longshore and cross-shore processes: The LX-Shore model. Environ. Model. Softw. 109, 1–16. https://doi.org/10.1016/j.envsoft.2018.08.010
Roelvink, D., Reniers, A., van Dongeren, A., van Thiel de Vries, J., McCall, R., Lescinski, J., 2009. Modelling storm impacts on beaches, dunes and barrier islands. Coast. Eng. 56, 1133–1152. https://doi.org/10.1016/j.coastaleng.2009.08.006
Roelvink, D.J.A., Meijer, T.J.G.P., Houwman, K., Bakker, R., Spanhoff, R., 1995. Field validation and application of a coastal profile model. Coast. Dyn. - Proc. Int. Conf. 818–828.
Scott, T., Masselink, G., O'Hare, T., Saulter, A., Poate, T., Russell, P., Davidson, M., Conley, D., 2016. The extreme 2013/2014 winter storms: Beach recovery along the southwest coast of England. Mar. Geol. 382, 224–241. https://doi.org/10.1016/j.margeo.2016.10.011
Splinter, K.D., Turner, I.L., Davidson, M.A., Barnard, P., Castelle, B., Oltman-Shay, J., 2014. A generalized equilibrium model for predicting daily to interannual shoreline response. J. Geophys. Res. Earth Surf. 119, 1936–1958. https://doi.org/10.1002/2014JF003106
Steetzel, H.J., 1995. Prediction of development coastline and outer deltas of Wadden coast for the period 1990–2040, WL Delft Internal Report H1887.
Stockdon, H.F., Holman, R.A., Howd, P.A., Sallenger, A.H., 2006. Empirical parameterization of setup, swash, and runup. Coast. Eng. 53, 573–588. https://doi.org/10.1016/j.coastaleng.2005.12.005
Stokes, C., Davidson, M., Russell, P., 2015. Observation and prediction of three-dimensional morphology at a high-energy macrotidal beach. Geomorphology 243. https://doi.org/10.1016/j.geomorph.2015.04.024
Turki, I., Medina, R., Coco, G., Gonzalez, M., 2013. An equilibrium model to predict shoreline rotation of pocket beaches. Mar. Geol. 346, 220–232. https://doi.org/10.1016/j.margeo.2013.08.002
Valiente, N.G., McCarroll, R.J., Masselink, G., Scott, T., Wiggins, M., 2019. Multi-annual embayment sediment dynamics involving headland bypassing and sediment exchange across the depth of closure. Geomorphology 343, 48–64. https://doi.org/10.1016/j.geomorph.2019.06.020
Van Rijn, L.C., 1993. Principles of sediment transport in rivers, estuaries and coastal seas. Aqua publications, Delft.
Villaret, C., Hervouet, J.-M., Kopmann, R., Merkel, U., Davies, A.G., 2013. Morphodynamic modeling using the Telemac finite-element system. Comput. Geosci. 53, 105–113. https://doi.org/10.1016/j.cageo.2011.10.004
Vitousek, S., Barnard, P.L., Limber, P., Erikson, L., Cole, B., 2017. A model integrating longshore and cross-shore processes for predicting long-term shoreline response to climate change. J. Geophys. Res. Earth Surf. 122, 782–806. https://doi.org/10.1002/2016JF004065
Warren, I.R., Bach, H.K., 1992. MIKE 21: a modelling system for estuaries, coastal waters and seas. Environ. Softw. 7, 229–240. https://doi.org/10.1016/0266-9838(92)90006-P

Yates, M.L., Guza, R.T., O'Reilly, W.C., 2009. Equilibrium shoreline response: Observations and modeling. J. Geophys. Res. 114, C09014. https://doi.org/10.1029/2009JC005359

Yates, M.L., Guza, R.T., O'Reilly, W.C., Hansen, J.E., Barnard, P.L., 2011. Equilibrium shoreline response of a high wave energy beach. J. Geophys. Res. 116, C04014. https://doi.org/10.1029/2010JC006681

k_1 {optimised}	k_2 {fixed}	r_c	r_v	$NMSE_c$	$NMSE_v$	CSS
0.0104	0.005	0.889	0.812	0.104	0.312	3.488
0.0108	**0.010**	**0.848**	**0.900**	**0.140**	**0.145**	**5.353**
0.0100	0.020	0.660	0.779	0.282	0.421	1.484
0.0095	0.040	0.444	0.529	0.401	1.153	0.307

Table 1. Model sensitivity analysis and skills scores for free parameters k_1 and k_2. k_1 is a response rate parameter which controls the magnitude of the morphodynamic variability and k_2 is a beach recovery parameter. Also shown are the Pearson correlation coefficients r for the calibration data (subscript c) and unseen validation periods (subscript v). *NMSE* is the normalised mean-square-error and *CSS* is a combined skills score defined in the text. The best results are highlighted in bold.

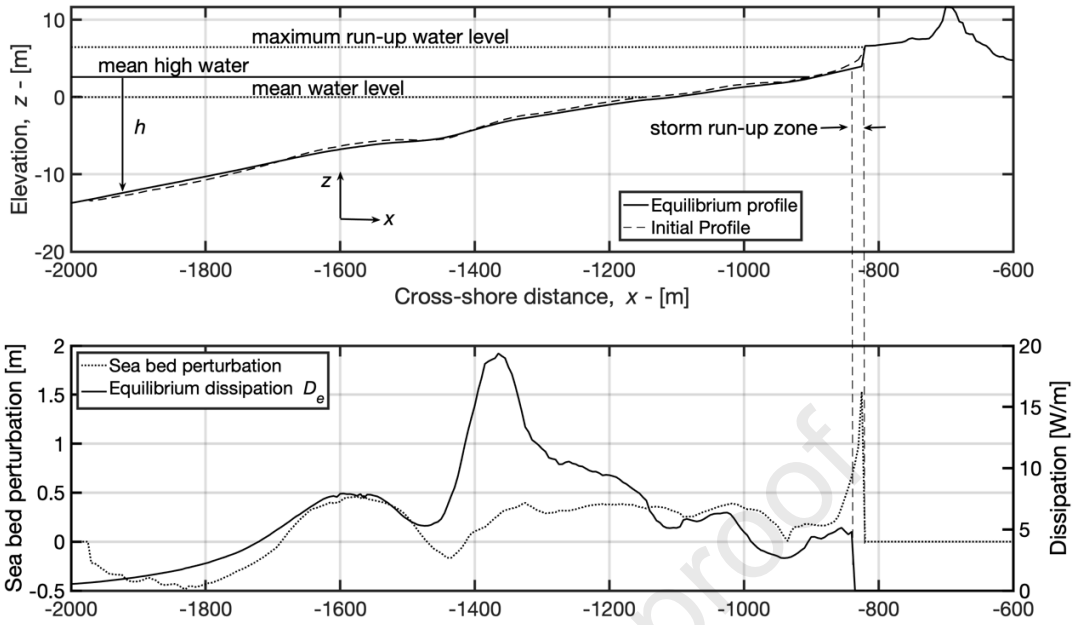

Figure 1. Top: Schematic diagram showing the model co-ordinate system, the equilibrium profile and initial model profile. Bottom: Figure showing the seabed perturbation, computed as the deference between the equilibrium and initial profile at t=0. Also shown is the equilibrium dissipation map D_e.

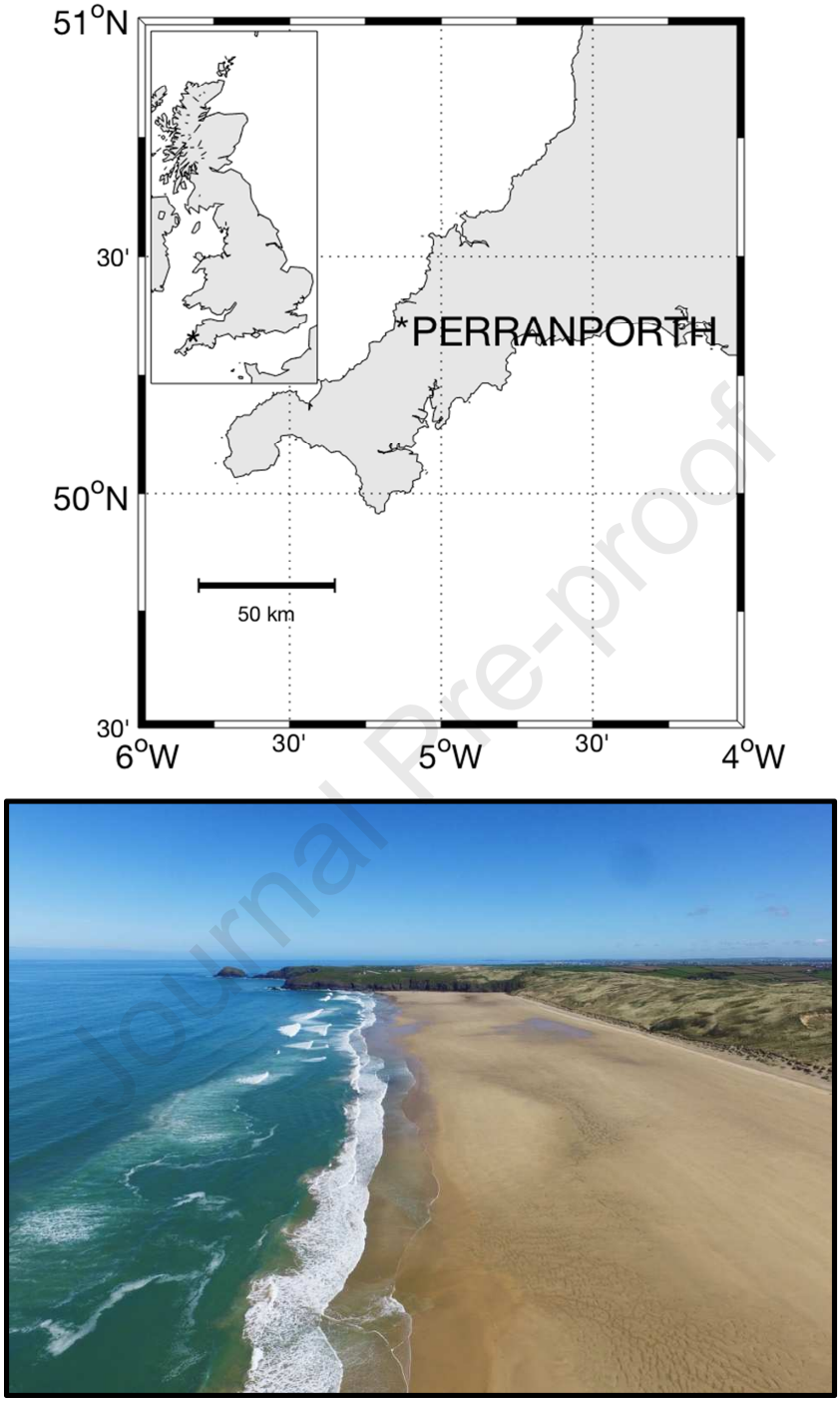

Figure 2. Top: Field site Location, Perranporth, UK, located on the north Cornwall coastline. Bottom: Aerial beach view showing coastal morphology. Notice the permanent offshore bar, highlighted by the breaking wave patterns. This is a low-tide image showing the broad intertidal area fronting a coastal dune system.

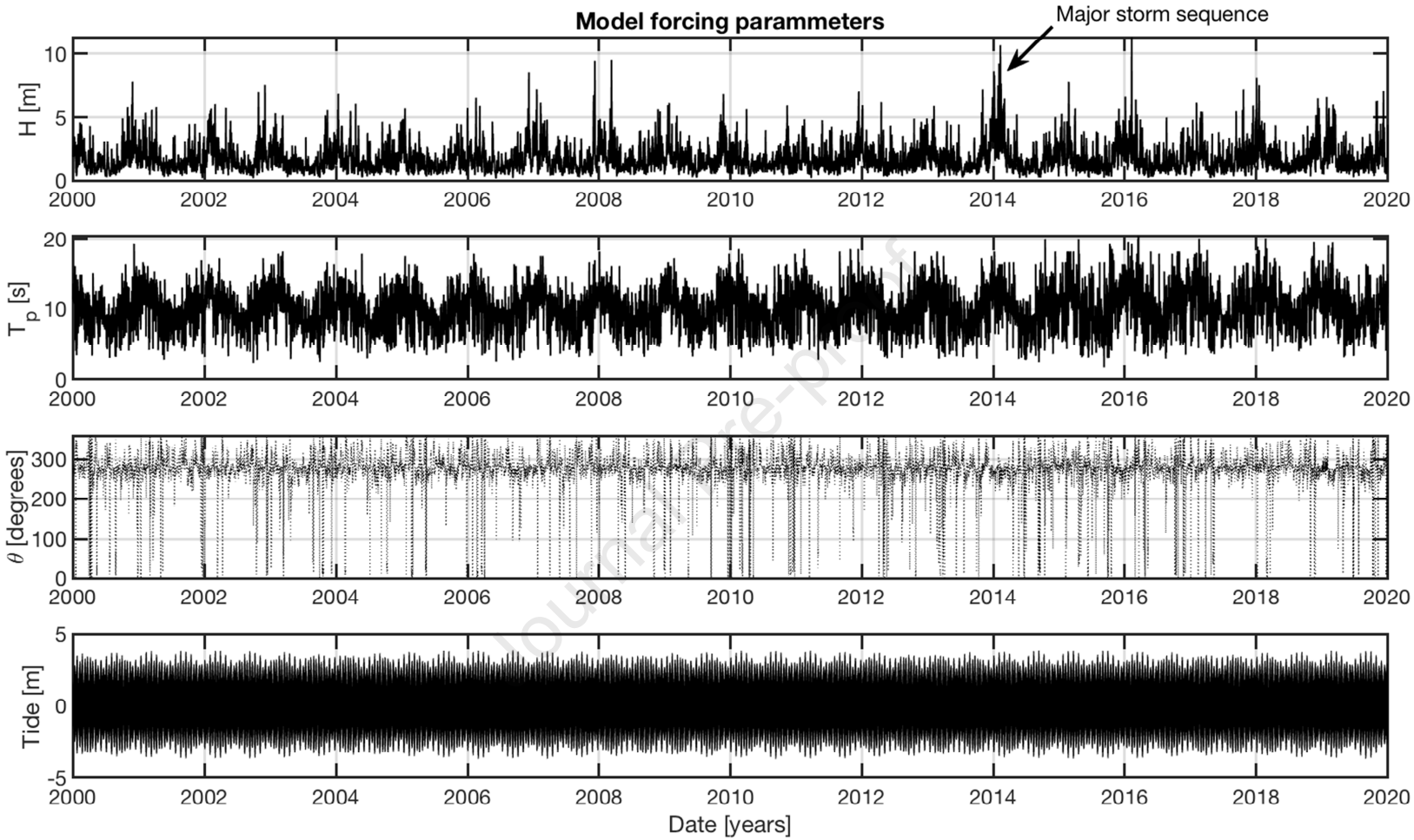

Figure 3. Model Forcing Parameters. Top three panels: Significant wave height, peak period and direction, all predicted in 17m water depth at Perranporth using the Met Office WWIII model. Notice the high seasonality in the incident wave parameters and the extreme storm event in 2013/14. Lower panel: Predicted tidal displacement for Perranporth.

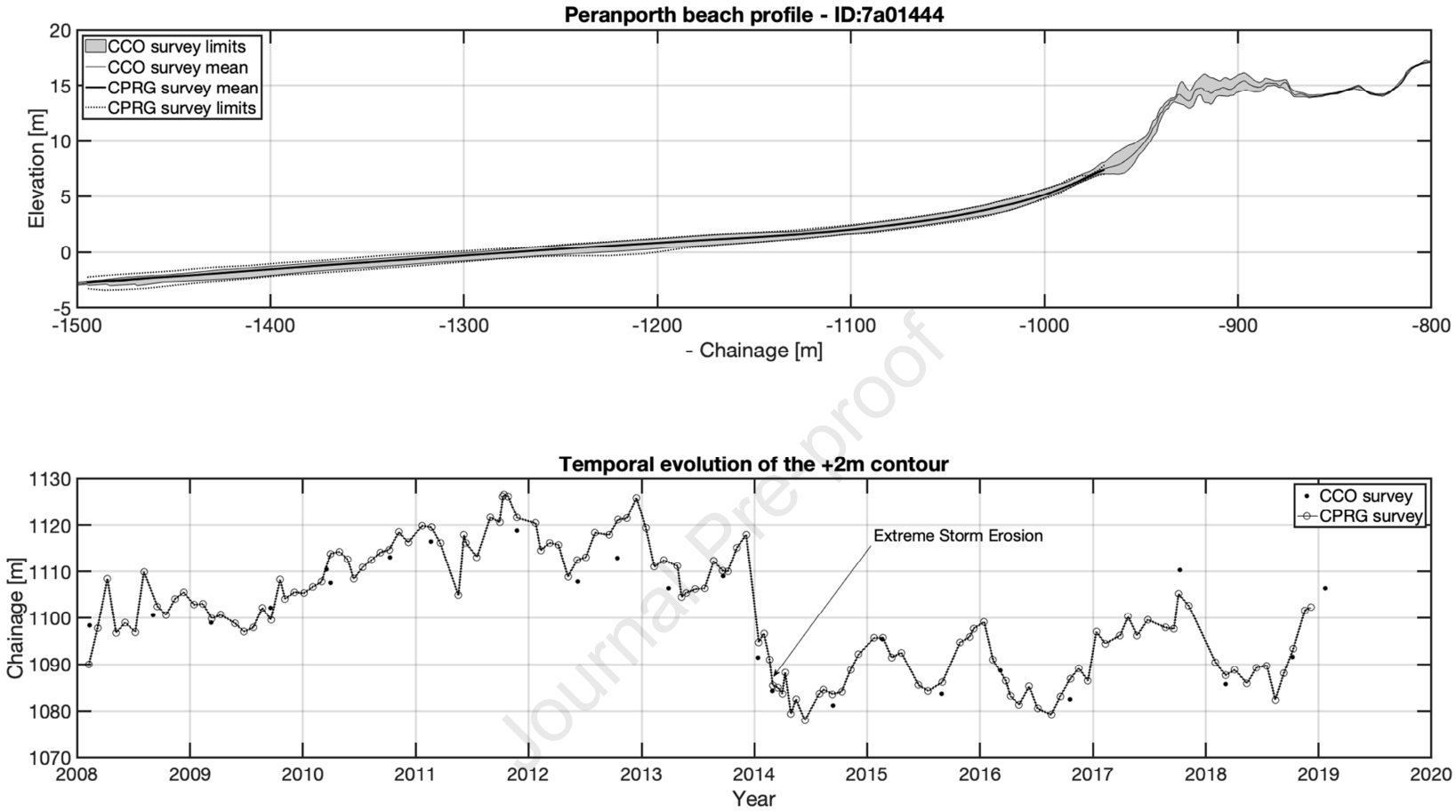

Figure 4. Perranporth beach surveys. Upper panel: Upper and lower limits of the beach surveys collected by the Channel Coastal Observatory (CCO, shaded area) and Plymouth University's Coastal Processes Research Group (CPRG, dotted lines) along profile line 7a0144 (CCO unique ID). The vertical reference is Ordinance Datum Newlyn. Lower panel: Cross shore location (chainage) of +2m contour at profile 7a01444. Results from both CCO and CPRG surveys are shown. Notice the seasonal and strong interannual signals in the shoreline behaviour and the extreme storm response in the winter of 2013/14.

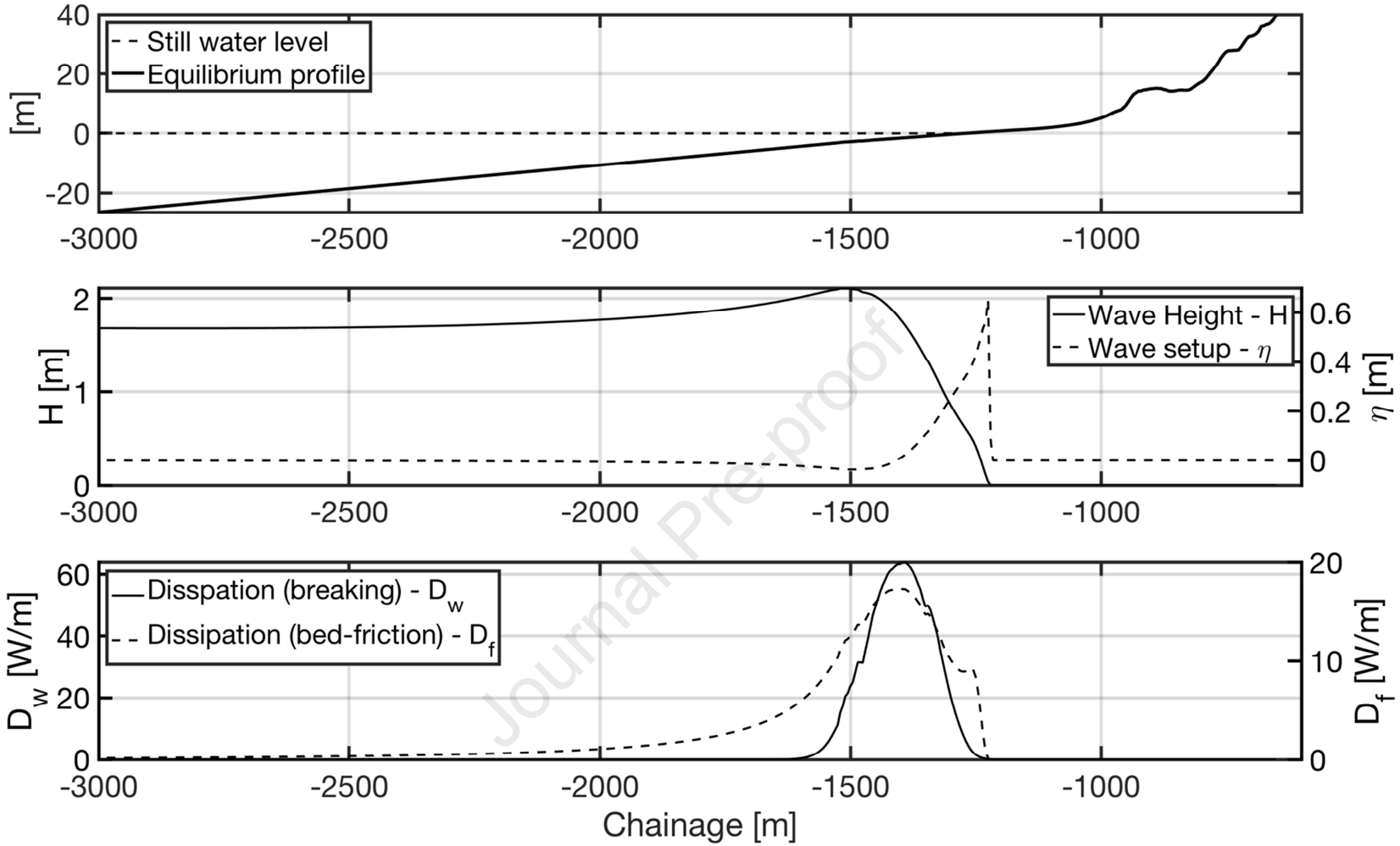

Figure 5. Model hydrodynamics: The upper panel shows the equilibrium beach profile used to initialise the ForCE model. The middle panel shows the evolution of the mean wave height and setup over the equilibrium profile. The lower panel shows the computation of wave dissipation due to both breaking and bed-friction, which are fundamental parameters used in the force model to predict sediment fluxes.

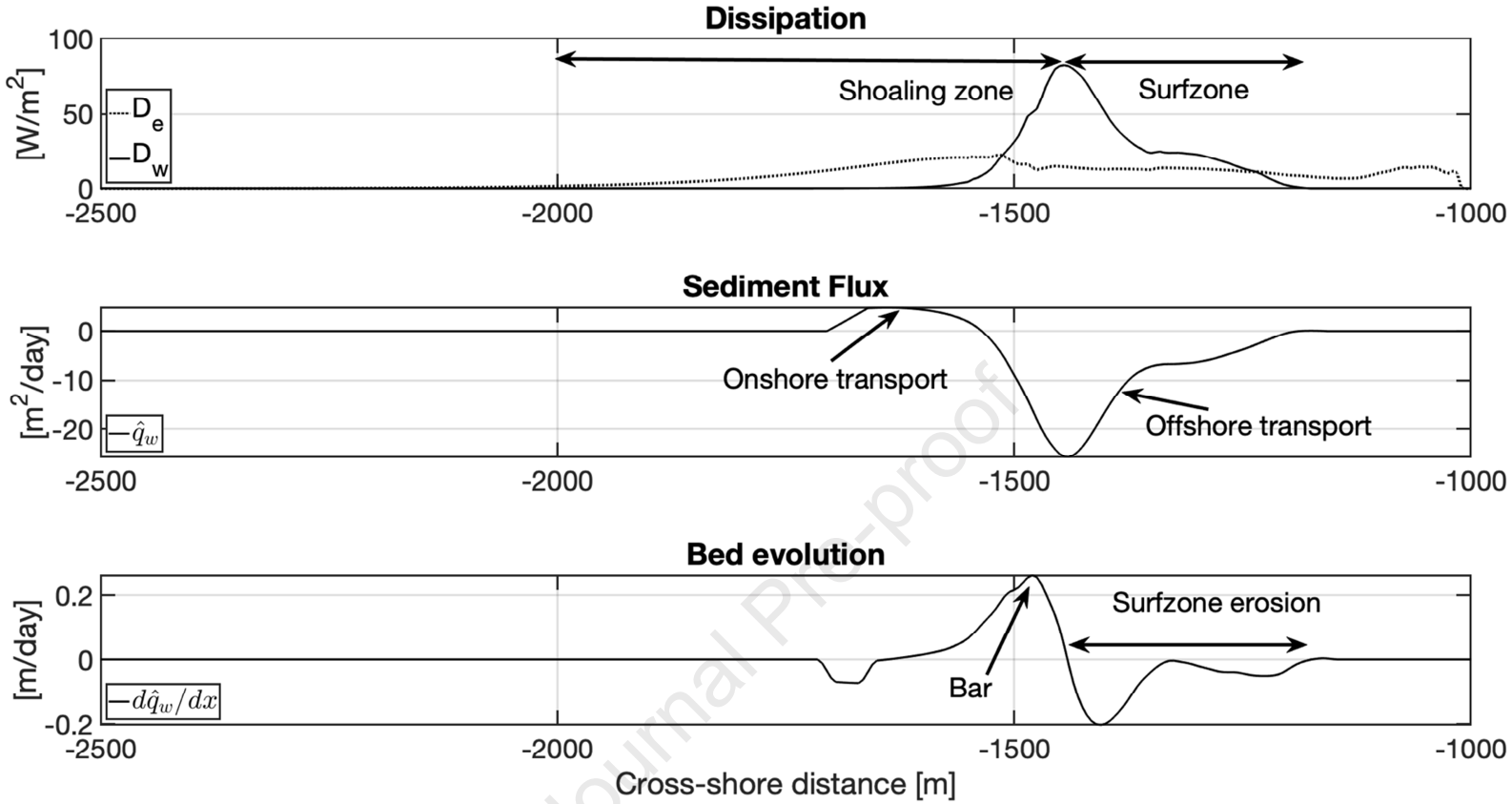

Figure 6. This plot shows the process of computing the sediment flux based on the disequilibrium in wave dissipation due to breaking (equation 15). Calculations are based on a mild storm condition, (H_s = 3 m). The upper panel shows the equilibrium dissipation map D_e (dotted line), which is a 5-year time-average of hourly wave dissipation profiles. Also shown is the instantaneous dissipation D_w (solid line). The flux calculation is shown in the middle panel. Notice that as $D_w < D_e$ in the shoaling zone but $D_w > D_e$ throughout the surfzone. This leads to onshore sediment transport in the shoaling zone (positive disequilibrium) and offshore transport (negative disequilibrium) in the surfzone. The lower panel shows the corresponding bed evolution given by the spatial divergence in the cross-shore sediment flux. Note the surfzone erosion and formation of a bar just seaward of the surfzone.

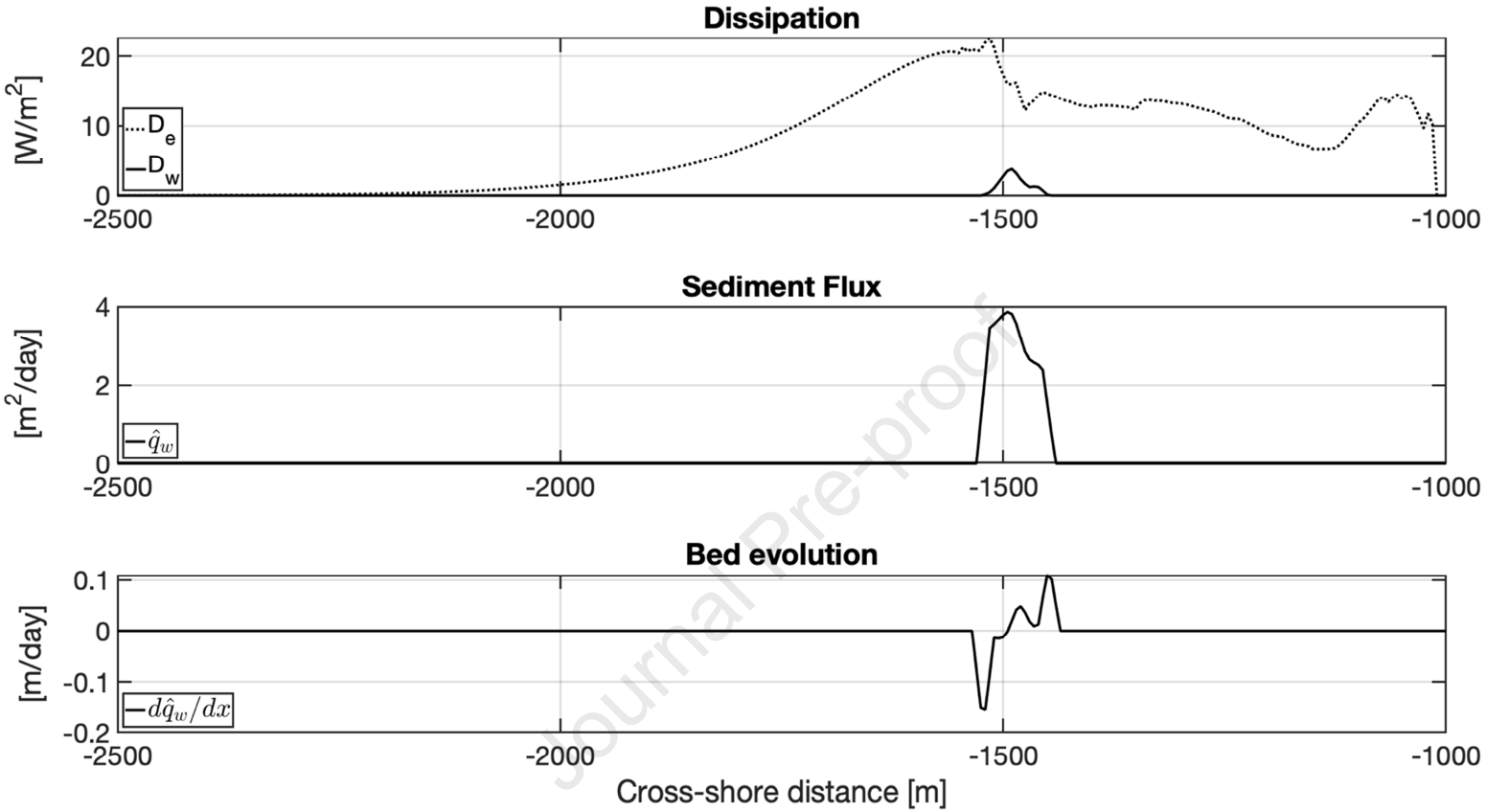

Figure 7. This plot shows the process of computing the sediment flux based on the disequilibrium in wave dissipation due to breaking (equation 15). Calculations are based on a mild (recovery) wave condition, (H_s = 0.5 m). The upper panel shows the equilibrium dissipation map D_e (dotted line) and the instantaneous dissipation D_w (solid line). The flux calculation is shown in the middle panel. Notice that as $D_w < D_e$ across the entire profile, leading to onshore sediment transport (positive disequilibrium) over the whole region of wave dissipation. The lower panel shows the corresponding bed evolution which mines sediment form pre-breaking shoaling zone and depositing it in the surfzone, contra to the prior storm example (figure 6).

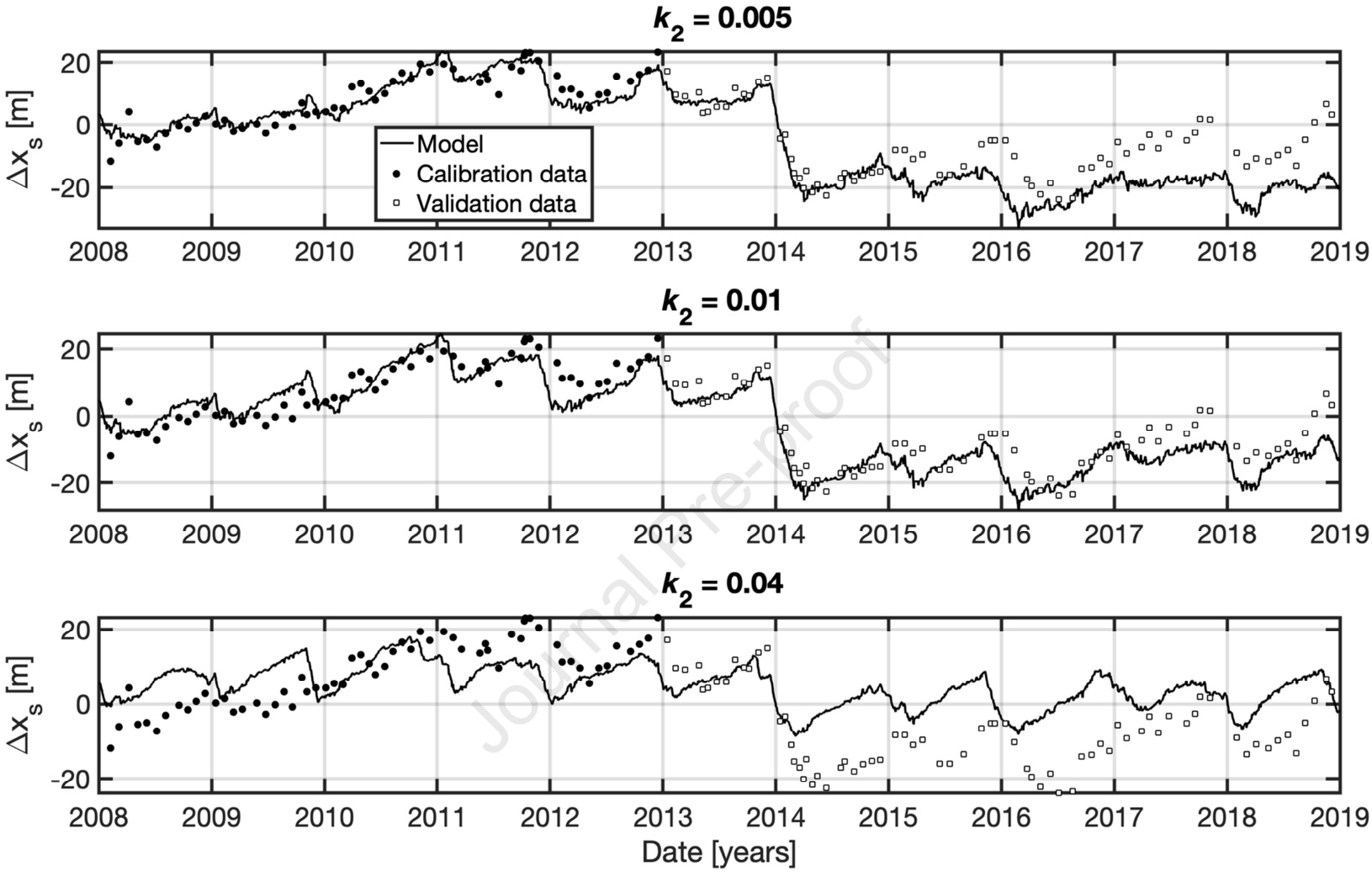

Figure 8. Model sensitivity analysis for the recovery coefficient, k_2. The plot shows model predictions (solid line) and measurements circles) of the temporal evolution of the z = 2 m shoreline contour. The closed circles represent the measurements which have been utilised for model calibration, whilst the open circles signify measurements unseen by the model. Notice that low values of the recovery parameter (top panel) lead to an underprediction of post storm recovery following the extreme 2013/14 storms, whilst high values (bottom panel), lead to a suppression of interannual variability and an over-prediction of beach recovery. Optimum results for are shown in the middle panel (k_2 =0.01). Note that the uncertainty in the shoreline measurements arising from longshore variability and interpolation errors is $\pm$4.27m.

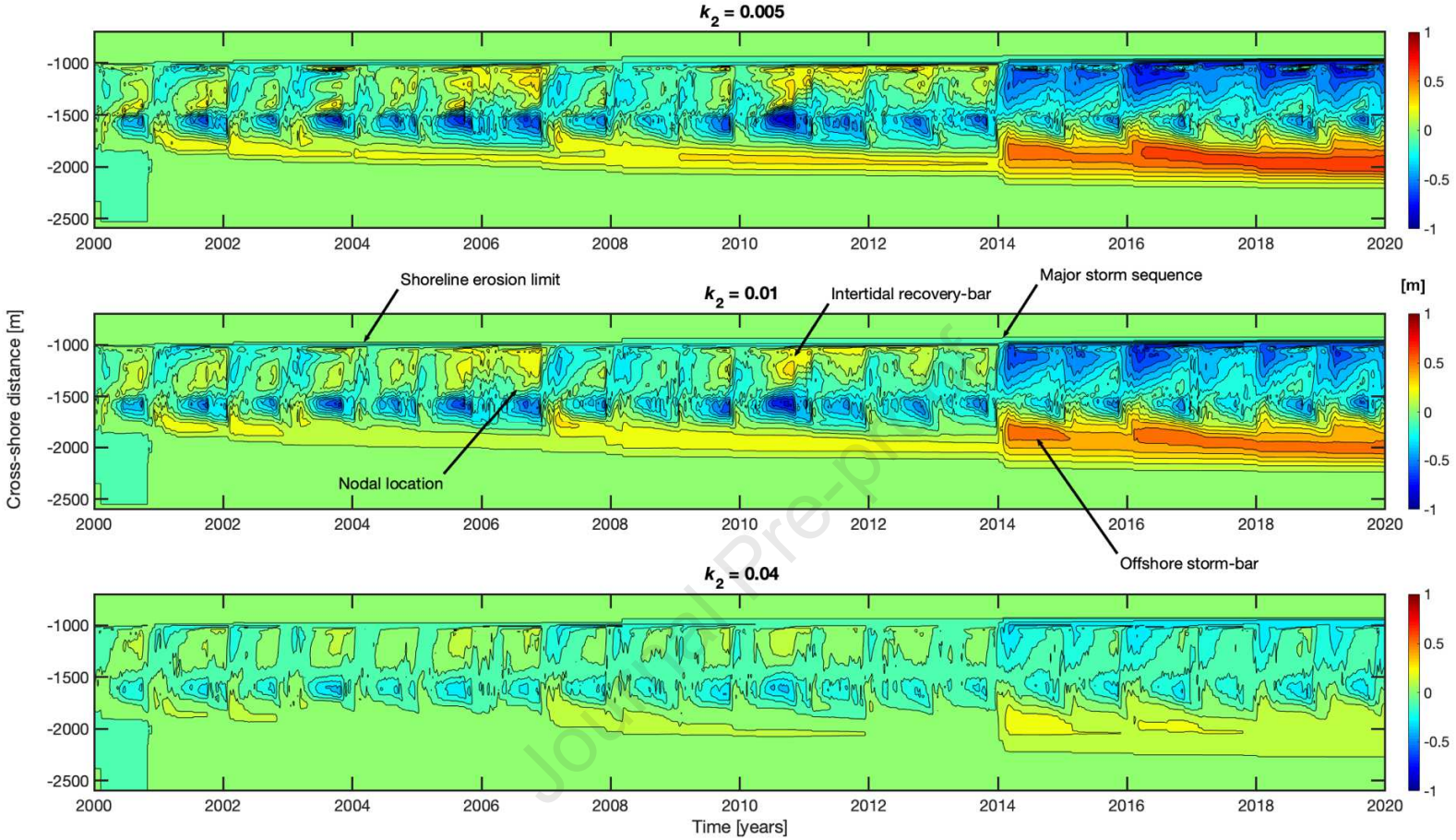

Figure 9. Plots showing the sensitivity of modelled profile evolution to the recovery parameter, k_2. With reference to the middle panel, notice how the model predicts the seasonal cycling of sediment between the shore-face and offshore region through a bed evolution node, located at $x \approx$ -1500 m. Surfzone erosion during winter (November-February) is synchronous with deposition offshore and the formation of a storm bar. In the recovery months (March-October) sediment is returned to the intertidal profile, first being deposited as an intertidal recovery bar, before advancing shoreward to recharge the intertidal profile. For optimum values of the recovery parameter (k_2), a persistent storm bar develops, which varies in magnitude temporally. Increasing the recovery parameter (bottom panel) reduces interannual variability and increases the speed of post-storm recovery and visa-versa (see top-panel).

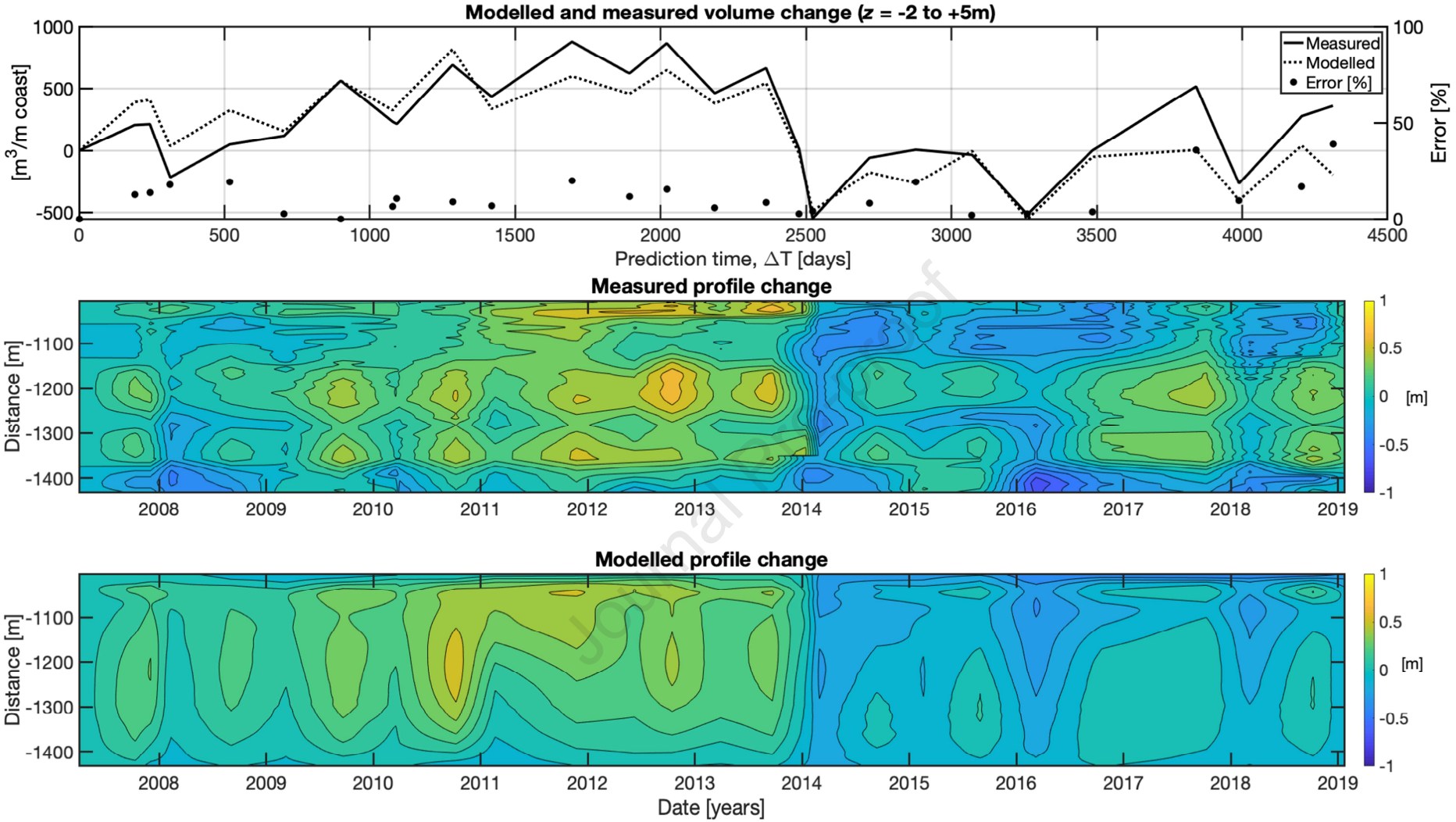

Figure 10. Comparison model intertidal-profile predictions (z = -2 to 5m) with equivalent unseen CCO surveys. Here the model profile evolution (lower-panel) has been extracted for the same survey times (middle-panel). The top-panel shows the cross-shore integration of the measured and modelled profiles to give the comparative volume change versus the prediction interval, ΔT. The error, expressed as percentage of the measured volume-range is also shown on the secondary y-axis.

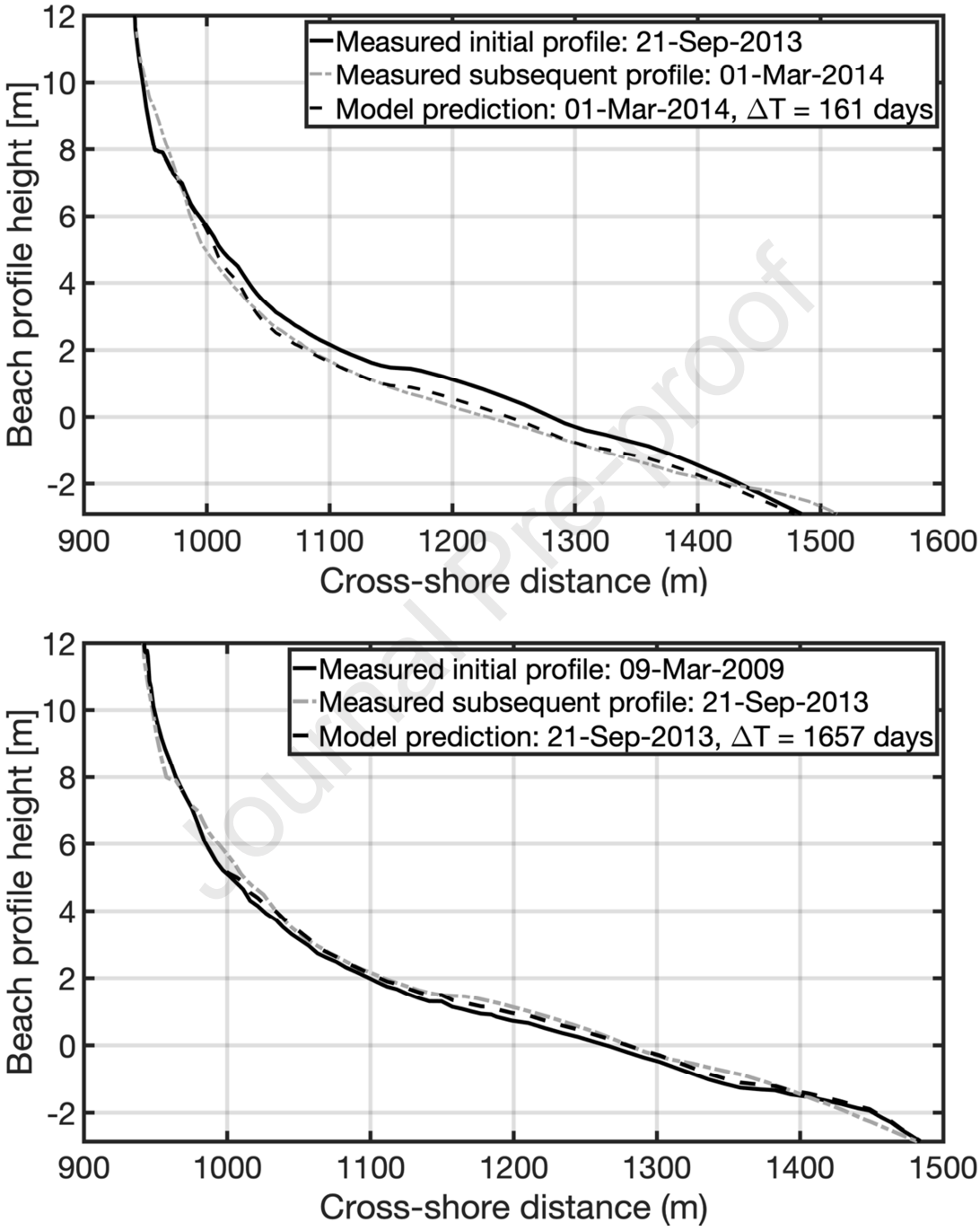

Figure 11. Example modelled and measured profile evolution for the extreme storm erosion in 2013/14 (top) and an extended multi-year accretional period between March 2009 and September 2013 (bottom).

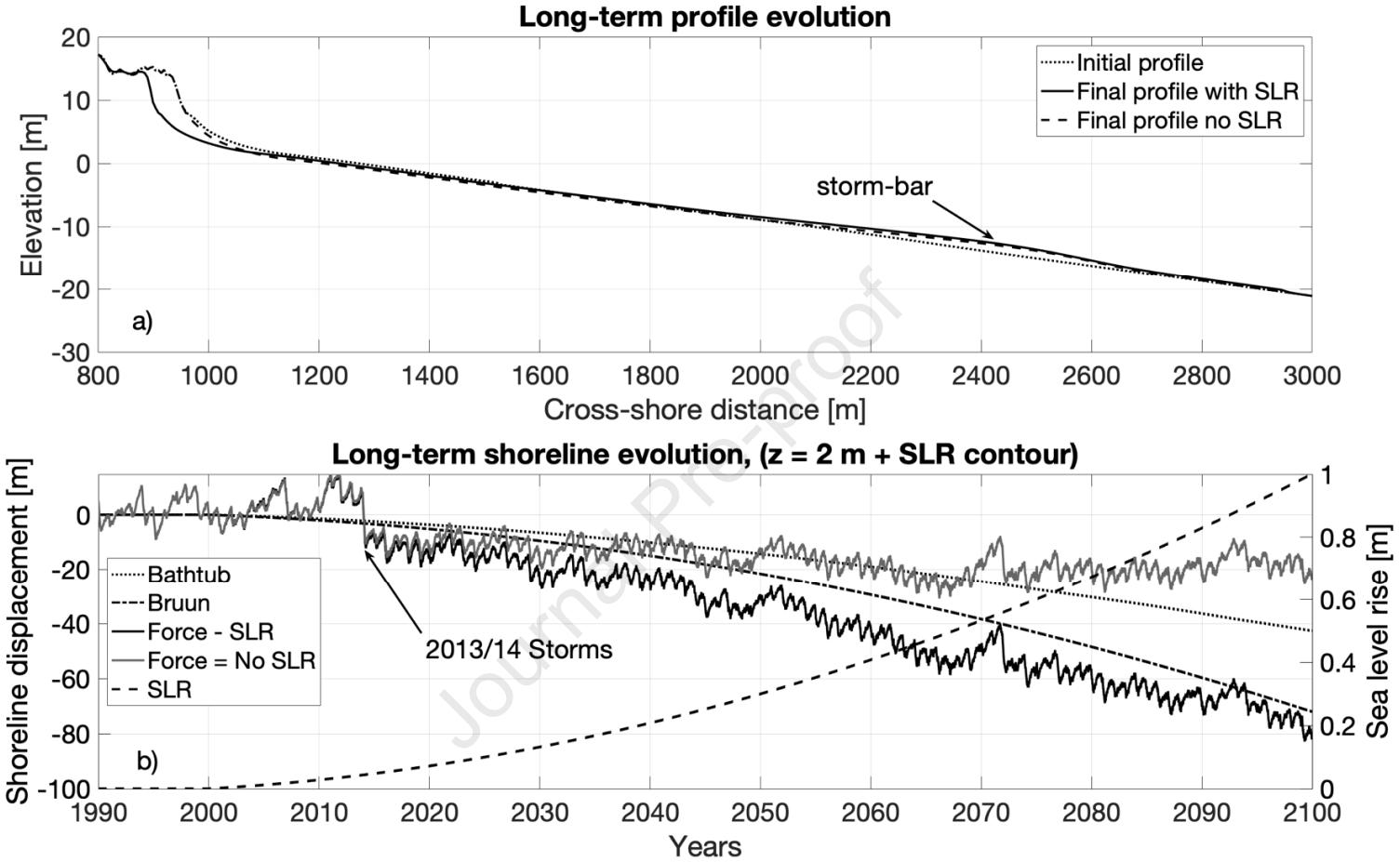

Figure 12. a) Initial and final beach profiles predicted after 110 years of simulation. Two model runs are included here, one without sea level rise and the other with 1m of sea level rise over the time-period 2000-2100. b) Evolution of the 2m + sea level rise shoreline contour, shown for both the with and without sea level rise model runs. Also shown here are the bathtub projections (no morphodynamic change) and Bruun-rule prediction. The modelled sea level rise is indicated on the secondary vertical axis.

k_1 {optimised}	k_2 {fixed}	r_c	r_v	$NMSE_c$	$NMSE_v$	CSS
0.0104	0.005	0.889	0.812	0.104	0.312	3.488
0.0108	**0.010**	**0.848**	**0.900**	**0.140**	**0.145**	**5.353**
0.0100	0.020	0.660	0.779	0.282	0.421	1.484
0.0095	0.040	0.444	0.529	0.401	1.153	0.307

Table 1. Model sensitivity analysis and skills scores for free parameters k_1 and k_2. k_1 is a response rate parameter which controls the magnitude of the morphodynamic variability and k_2 is a beach recovery parameter. Also shown are the Pearson-correlation coefficients r for the calibration data (subscript c) and unseen validation periods (subscript v). *NMSE* is the normalised mean-square-error and *CSS* is a combined skills score defined in the text. The best results are highlighted in bold.

Highlights: Predicting morphodynamic evolution on time-scales of days to decades

By Mark Davidson

1. Days to decades prediction of coastal evolution
2. Accurate predictions of storm erosion & post-storm beach recovery
3. Skilful long-term prediction of beach volume and shoreline change & bar-dynamics
4. Explicit consideration sub- and supra- tidal topography & water level
5. Stable, efficient, equilibrium model suitable for longterm probabilistic forecasts